Musculoskeletal modelling of the shoulder during baseball pitching

A research combining 3D kinematic measurements with musculoskeletal modelling

By

Peter Hordijk BSc. Mechanical Engineering

in partial fulfilment of the requirements for the degree of

Master of Science
in Biomedical Engineering

at the Delft University of Technology,
to be defended publicly on Tuesday August 22, 2017 at 15:00

Supervisor:	dr. X. Gasparutto	
Thesis committee:	Prof. dr. H.E.J. Veeger	TU Delft
	Prof. dr. F.C.T. van der Helm	TU Delft
	Dr. A.A. Zadpoor	TU Delft.

TU Delft

Table of contents

1 Introduction

Baseball belongs to the most popular and commercial sports in the world. In their search for improvement, coaches often seek the help of science. Not only is a lot of effort done trying to make pitchers throw faster, but injury prevention is also a major concern. Indeed, premature career endings are omnipresent among pitchers due to injury in the throwing arm. The science of biomechanics can aid coaches in this process, using powerful tools like motion analysis and musculoskeletal modelling. The Dutch royal baseball and softball federation (KNBSB) supports such research in the project 'FASTBALL' (Fast And Safe Throwing in baseball), a collaboration between the Vrije Universiteit Amsterdam and Delft University of Technology. The research in this thesis is part of this project.

Pitching is a complex motion involving many joints and requires coordinated movement patterns to transfer energy from the legs via the trunk and throwing arm to the ball. The motion can be divided in the windup, stride, arm cocking, acceleration, deceleration and follow-through (Werner et al., 1993), as illustrated in Figure 1.

In the windup, the ball is still in the glove and the pitcher prepares a fitting starting position, which varies a lot per person. The windup involves lifting the non-dominant leg, called the striding leg. Striding starts with taking the ball out of the glove, stepping towards the home plate with the striding leg and ends with the foot contacting the pitching mound. In arm cocking, the throwing hand is moved back as much as possible. This is achieved by humeral external rotation, shoulder abduction, elbow flexion and scapular retraction (Seroyer et al., 2010, Moynes et al., 1986). At this moment, hand and ball have minimal velocity, and acceleration starts. The scapula is protracted, the humerus is rotated internally and adducted horizontally. In the acceleration phase, a lot of power is produced and a high shoulder internal rotation speed of sometimes over 9000°/sec is reached (Pappas et al., 1985, Fleisig et al., 1999). After ball release deceleration starts. The follow-through is used to put the body in a balanced position again. This is mainly done using the trunk and lower body.

This thesis will deal with applying a musculoskeletal model to the pitching motion. Such a model makes it possible to estimate the muscle forces and joint loads. This will give insight in the understanding of shoulder mechanics during pitching and is assumed to improve performance and understanding of injury mechanisms. A model of the shoulder region will be used, because the shoulder plays such an important role in pitching. A number of 3D models of the shoulder region are available, varying in complexity and the anatomical data used. Examples are the Swedish model (Karlsson and Peterson, 1992), SIMM (Holzbaur et al., 2005), the AnyBody model (Damsgaard et al., 2006) and the Newcastle model (Charlton and Johnson, 2006). Among the most sophisticated models is the Delft Shoulder and Elbow Model (DSEM). In this research the DSEM will be used, because it is advanced, and because of the expertise on this model available at our university. Our goal is to use simulations of the pitching motion in the DSEM to study the motion. Currently, there are three problems that impede proper simulations.

The first problem is the lack of proper kinematic recordings, especially as the scapula is difficult to track due to the high amount of soft tissue covering it, its flat shape and the amount of skin deformation during motion. The second problem is the fact that the model is based on the muscle properties of an elderly man. Accordingly, the maximum force of the model could be too limited to generate the high accelerations that occur in the pitching motion. The third problem is the extreme character of the motion: higher bone velocities and larger bone rotations occur compared to previous simulations in the DSEM. Additionally, pitchers have an adapted range of motion (Brown

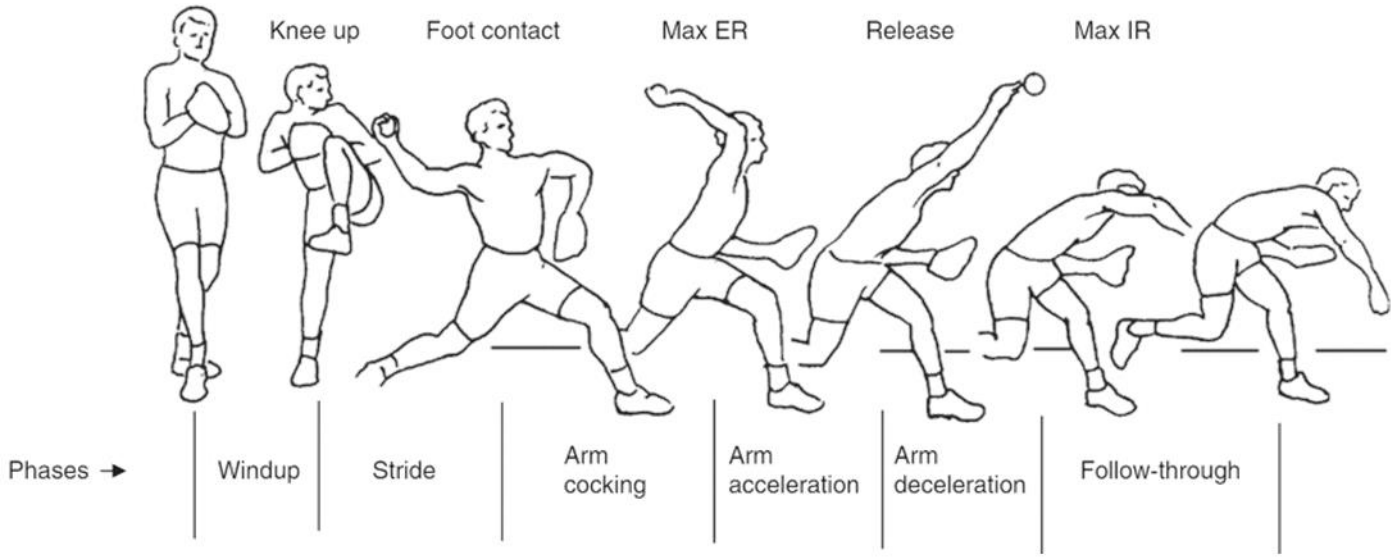

Figure 1: Phases of the pitching motion. ER: external rotation. IR: internal rotation. Adapted from Fleisig et al. (1996)

et al., 1988, Ellenbecker et al., 2002), which may cause incompatibility with the model.

An experimental study will be performed to address these problems, combining kinematic measurements, including tracking of the scapula, with force measurements. This will result in a dataset that can be used as an input for the DSEM, where the kinematic data can be used as an input and the force measurements can be used to scale the maximum force of the model. Consequently, in a simulation study the DSEM will be used with these data to study the compatibility of the kinematic data with the model and the effects of force scaling.

Finally, the motion will be studied. Knowledge of the musculoskeletal interactions that result in the high accelerations that occur in pitching is lacking. The kinematic model of the DSEM will be used to estimate muscle length and velocity to give information about the contribution of individual muscles during the motion.

2 Measuring pitching kinematics and maximum force to provide a dataset for a musculoskeletal model

An experimental study

2.1 INTRODUCTION

A musculoskeletal model of the shoulder region can be used to study the baseball pitching motion, because it estimates muscle forces and joint loads, which give valuable information. This will give insight in the understanding of shoulder mechanics during pitching and is assumed to improve performance and understanding of injury mechanisms. For simulation in such a model, kinematic data of the upper limb during the pitching motion is required. Additionally, it might be necessary to scale the maximum force of the model, since this might be too limited to generate the high segment accelerations that occur in the pitching motion of elite pitchers. To allow for scaling, it is required to measure the maximum force of pitchers. An experimental study will be performed, combining shoulder kinematic measurements during pitching with maximum force measurements, to deliver a dataset that can be used for simulations of the pitching motion in a musculoskeletal model of the shoulder region.

2.1.1 Pitching kinematics

Shoulder kinematics have already previously been measured using a maker-based method (Fleisig et al., 1996) and with video analysis (Dillman et al., 1993). However, there have been no reports of measurements of all the joints in the shoulder region using either method. Besides the glenohumeral joint, these include the scapulothoracic gliding plane, the sternoclavicular, and acromioclavicular joints, which are all linked.

Generally, arm segment rotations are often estimated by the thoracohumeral motion, neglecting the scapulothoracic motion. The scapula, however, plays an important role in the pitching motion. It stabilizes the glenohumeral joint, protracts and retracts around the thorax, and is an important link in kinetic energy transfer which takes place during the late cocking to the acceleration phase from the proximal to the distal segments (Kibler, 1998). While for general approximations a thoracohumeral description of arm segment rotations might be sufficient, for pitching it is desirable to include measurements of scapular motion because of its important role.

While measurement of scapular motion is common for daily life activities (van Andel et al., 2008), shoulder pathologies (Lopes et al., 2015), and some sports (Veeger et al., 1993, Prinold and Bull, 2016), no reports appear to be available on scapular motion recordings during pitching. Measuring scapular motion is difficult due to the high amount of soft tissue covering it, its flat shape and the amount of skin deformation during motion, which would be especially high in an explosive task like baseball pitching. These problems make the use of cutaneous markers, which is common for motion capturing, problematic to track the scapula.

Besides cutaneous markers, there are a number of methods available to measure or estimate scapular motion in 3D: scapulohumeral regression (Veeger et al., 1993, de Groot and Brand, 2001), using a scapula locator (Johnson et al., 1993, Meskers et al., 1998, Barnett et al., 1999, Masjedi and Johnson, 2011), digital fluoroscopy (Talkhani and Kelly, 2001, Mandalidis et al., 1999), stereophotometry (Jacq et al., 2010), the moiré method (Gomes et al., 2010), a marker-based skin deformation method (Brackbill et al., 2007) and using a skin-mounted acromion tracker (Karduna et al., 2001, Meskers et al., 2007, van Andel et al., 2009). The decision on what scapula tracking method to use can have large impact on following simulation studies, because the sensitivity of musculoskeletal model predictions for scapula angles is very high. This is caused by the fact that the orientation and displacement of the scapula have a large influence on the moment arms of attaching muscles (Happee and Van der Helm, 1995, Charlton and Johnson, 2006). This is because movement of the scapula changes the perpendicular distance of the muscle line of action to the joint rotation center for attaching muscles.

In this study, scapular motion will be tracked using a skin-mounted acromion tracker, as recommended by Lempereur et al. (2014) and used by Karduna et al. (2001), Meskers et al. (2007) and van Andel et al. (2009), as the other methods are not applicable for pitching. Most important considerations for this are its accuracy and the fact that the pitching motion is a multiplanar, highly dynamic motion and should not be constrained by the measurement method.

2.1.2 Scaling force in a generic model

A musculoskeletal model of the shoulder region can be used to estimate muscle forces and joint reaction forces during the pitching motion. When a musculoskeletal model is used for a task with high segment velocities and accelerations such as baseball pitching, high muscle forces are required and the maximum force of the model might be too limited. High muscle forces are required because of Newton's second law of motion and because of the force-velocity relationship of muscles, stating that muscles are able to produce submaximal force at high contraction velocities. However, the force-velocity relationship would only be a factor in theory for pitching, because it has not been implemented in the inverse-dynamics model of the DSEM (Nikooyan et al., 2011). Since more force

might be required, scaling of the muscle properties is appropriate.

The DSEM is a generic model created from measurements obtained from a 57-year old cadaver (Nikooyan et al., 2011). The use of a generic model makes it possible to study the musculoskeletal behavior of anyone by only measuring their joint angles during a certain motion. Moreover, many anatomical parameters that are required for modelling are impossible to measure in vivo. However, the use of a generic model also has disadvantages. There is a discrepancy in the anatomical and physiological musculoskeletal parameters between the elderly man whose cadaver is modelled and the subjects that participate in kinematic measurements, which are young athletes. This can result in the muscle force being too low in the model to perform a simulation. This problem doesn't occur for daily life activities, in which the DSEM has predominantly been used, because of the fact that these motions didn't require very high segment accelerations or high external force. For such motions, the muscle forces will not approach their limits and force scaling isn't required despite possible differences in force between subjects and the model. In contrast to daily life activities, in baseball pitching high segment accelerations occur, which require high muscle forces. Accordingly, the maximum muscle forces in the model might be too limited to generate the high segment accelerations, therefore making scaling essential.

The difference between the maximum force of the model and of the pitcher can be compensated for by scaling maximum force, and more specifically by scaling physiological cross-sectional area (PCSA). PCSA is defined as the area of the muscle perpendicular to the muscle fiber direction. PCSA is one of the musculoskeletal parameters obtained from a cadaver to base the generic model on, as well as muscle fiber length, pennation angle and joint rotation center (Veeger et al., 1997). PCSA is assumed to relate to the maximum muscle force linearly (Bamman et al., 2000, Fukunaga et al., 2001). This has also been assumed in the DSEM, where the following relationship is implemented to calculate the maximum muscle force (F_{max}):

$$F_{max} = f(l_{mus}) * PCSA * \sigma_{max}$$

Here $f(l_{mus})$ is the normalized force-length relationship and σ_{max} is the maximum muscle stress of the muscle.

To compensate for the difference in force of a subject and the modelled cadaver, it is possible to scale the PCSA in a musculoskeletal model. It makes sense to do so, since muscle volume, which is linearly related to PCSA by dividing by optimum fiber length, differs greatly between individuals (Vidt et al., 2012).

PCSA scaling has been performed by Bolsterlee et al. (2015) using two methods: First, PCSA of all muscles was scaled using a single factor derived from maximum force measurements. This approach takes inter-individual differences in muscle volume into account, but neglects a difference in distribution of muscle volume among muscles. Second, PCSA was scaled with an individualized scaling factor for all the muscles, with muscle volume derived from MRI measurements. In contrast with the first method, this method takes into account the difference in distribution of muscle volume. However, little difference was shown between the results of the two methods, which means that the effect of muscle volume distribution and thus force distribution over muscles is only marginal. Accordingly, in this study an attempt will be made at scaling the maximal force of the model with only a single scaling factor, which can be obtained with a simple measurement procedure. This scaling method can be regarded as successful when the method will result in sufficient muscle force in a simulation of the pitching motion. However, this could also be achieved without force measurements and simply using a very high scaling factor. Therefore, in addition the scaling factors found must actually represent a difference in muscle force between the subject and the model. Whether or not the muscle force will be sufficient for pitching will be studied in a simulation study, which can be found in Chapter 3.

2.2 METHODS

2.2.1 Subjects

The subjects of the kinematic and force measurements were Dutch AAA level pitchers (n = 19), age 15.9 ± 0.74 year, height 185 ± 7.6 cm, and of 75.2 ± 10.0 kg. After having been informed of the aims and procedures of the experiment, all players and/or their legal representatives signed an informed consent form. The VU Faculty of Human Movement Sciences' local ethical committee approved this research project.

2.2.2 Kinematic measurements

3D kinematic data were recorded using a marker based optoelectronic measurement technique. Eight cameras (140Hz) were used, which were a combination of Optotrak Certus and Optotrak 3020 cameras (Optotrak, Northern Digital Inc., Canada).

The subjects wore a tight shirt and all the markers were taped to the shirt at the location of a bony landmark. They were equipped with twelve active LED markers on the following positions: three markers on the thorax cluster and on the side of the throwing arm on the medial humeral epicondyle (EM), lateral humeral epicondyle (EL), ulnar styloid US), radial styloid (UR), head of the third metacarpophalangeal joint (RHIP3) and four markers on the acromion cluster. The markers

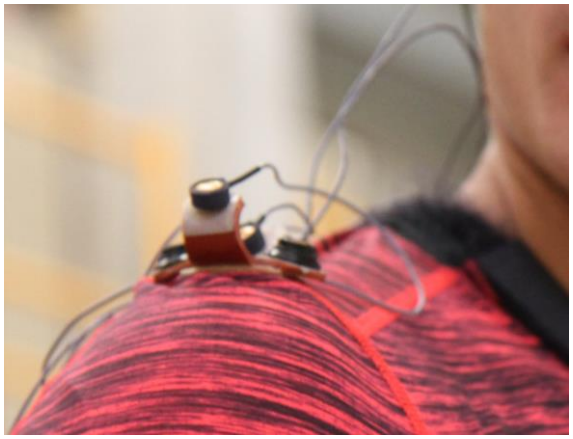

Figure 2: Acromion cluster

on the acromion cluster, shown in Figure 2, were connected rigidly to each other by a frame. Two markers are facing upwards, two markers are facing laterally with 45° upward tilt. Three markers are required to describe the three degrees of freedom of the scapula. Four markers were used for the cluster to increase the number of frames where at least three markers were visible. The cluster was taped to the flat part of the acromion. The cluster weighed $1*10^2$ g and the size of the base was 10x10 mm.

The following anatomical landmarks were pointed to measure their relative position with respect to the thorax cluster and reconstruct their motion: spinous process of the 7th cervical vertebra (C7), insicura jugularis (IJ), xiphoid process (PX), spinous process of the eight thoracic vertebra (T8). The following anatomical landmarks on the scapula were palpated with a pointer to measure their relative position to the acromial cluster: angulus acromialis (AA), trigonum spinae (TS), angulus inferior (AI), acromioclavicular joint (AC). The anatomical landmarks on the scapula were palpated with a pointer in anatomical position and four key upper limb configurations of pitching: windup, maximal external rotation, ball release and end of follow-through. The average position of the markers expressed in the acromial cluster was used to reconstruct the trajectory of the scapula landmarks. A synchronized high speed camera (240 Hz), located at the side of the throwing arm facing the pitcher, was used to determine the instant of ball release. The camera was also used to check whether the acromion cluster stayed in place relative to the acromion, by looking at whether or not the base of the cluster was parallel to the acromion from this side view. A speed gun was used to determine the ball velocity and a target was used to determine whether the pitch was a strike or a ball. After a warm-up of 20 to 30 minutes, the subject performed a total of 5 pitches, after being instructed to throw a fastball at maximum speed at the target.

Pearson correlation coefficients were generated to determine the relationship between maximum ball velocity and age, height and weight using Matlab (version 2014a, Mathworks). Statistical significance was set a priori at $P < 0.05$.

The 3D coordinates of the markers were filtered using a low-pass fourth order Butterworth filter with a cut-off frequency of 12.5 Hz and then converted to joint angles using ISB recommendations (Wu et al., 2005). The bony segment coordinate systems of the thorax, clavicle, scapula, humerus and lower arm were defined in accordance with the ISB recommendations, with the following exceptions: for the clavicle, the IJ was used instead of the most ventral point on the sternoclavicular joint (SC), because this would have required an extra marker, which would have lowered the sampling frequency. For the humerus, the following coordinate system was used: the y-axis was the line connecting the glenohumeral joint rotation center (GH) with the midpoint of EL and EM, pointing proximally. The x-axis was the line perpendicular to the plane formed by GH, EL and EM, pointing forward. The z-axis was the common line perpendicular to the x- and y-axis, pointing to the right. For the hand, the following coordinate system was used: the y-axis was the line connecting RHIP3 and the midpoint between US and RS, pointing proximally. The x-axis was the line perpendicular to the plane through US, RS and RHIP3, pointing forward. The z-axis was the common line perpendicular to the x- and y-axis, pointing to the right. The glenohumeral joint rotation center was found using linear regression, as described by Dumas et al. (2007). Joint angles were estimated from the marker coordinates for the following joints: thorax relative to the global coordinate system, the position of the IJ, clavicle relative to the thorax, scapula relative to the thorax, humerus relative to the thorax, lower arm relative to the humerus and hand relative to the lower arm.

2.2.3 Force measurements and scaling

The maximum force in six directions of the subjects was found by maximum voluntary contraction measurements over time on a handle with an AMTI SRMC3A 6 axis force transducer (200Hz) (Advanced Medical Technology Inc., USA) attached to it. The subjects were positioned on a stool and were instructed to hold on to a handle and to keep their elbow flexed 90° and the forearm pronated 90°, as shown in Figure 3. Then the subjects were instructed to apply maximum force with their arm on the handle in six directions consecutively: pushing, pulling, left, right, upward and downward, without using their trunk. A pause of 2 seconds was observed between each direction. This sequence was repeated three times. For each direction, the highest attempt of the three was taken as their maximum force. Appendix 7.1 describes how the raw data were converted to force in N.

The maximum force of the model was found by performing six simulations in the DSEM (version 4.2 in Fortran). The position of the subjects was not recorded, thus for the input kinematics an estimated position was created for each subject with the elbow flexed 90° and the forearm pronated 90° for all frames. This was the position in which subjects performed the force measurements as well. During the simulation, the external force on the hand was increased linearly in one direction at a time, with the other external forces remaining zero until the maximal force allowed by the model was reached. These six directions of external force corresponded to the six directions of

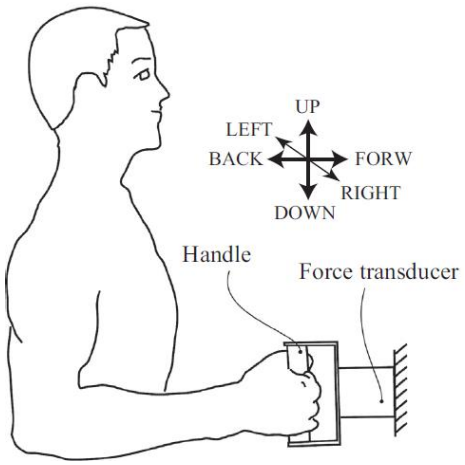

Figure 3: Measurement position (Bolsterlee et al., 2015)

the force measurements. The maximum force of the subjects was divided by the maximum force of the model for each direction. The highest value of these six was used for the scaling factor for each subject to ensure that the model was able to reproduce the force of the subject in all directions, which would not be the case when taking the mean of all six directions.

2.3 Results

2.3.1 Kinematic measurements

3D coordinates of twelve bony landmarks in the shoulder region were recorded for 115 throws from 19 subjects, along with ball velocity and strike or ball registration. Ball velocity ranged from 60 to 80 mph and was on average 74.1 ± 3.7 mph. Number of strikes thrown out of 5 was on average 2.7 ± 1.2 times. Ball velocity range and mean in mph and number of strikes are shown for all subjects along with their age, height and weight in Table 1.

A non-significant negative correlation ($r = -0.133$, $r^2 = 0.018$, $P = 0.588$) was found for the relationship between maximum ball velocity and age. A very weak positive correlation ($r = 0.0504$. $r^2 = 0.003$, $P = 0.838$) was found for the relationship between maximum ball velocity and height. A moderate positive correlation ($r = 0.410$, $r^2 = 0.168$, $P = 0.081$) was found for the relationship between maximum ball velocity and weight. None of the correlations found were statistically significant. The results of the correlation analyses can be found in Table 2.

To create a kinematic dataset to be used in a musculoskeletal model of the shoulder, bone rotations were calculated from the markers for 5 throws for subject 18 (15 years, 169 cm, 51 kg). Pitching velocity for this subject was on average 67.8 ± 0.84 mph (Table 1). The rotations of the clavicle, scapula and humerus are shown in Figure 5 for one representative pitch. The mean maximal values of angles between scapula and thorax are shown in Table 3.

The clavicle was elevated during the entire pitch and was elevated the most in the acceleration phase. There was no protraction of the clavicle, but retraction was large in the cocking phase. The main motion of the scapula was from retraction in the cocking phase to protraction in the acceleration phase, which was on average 6° and 71° respectively. Forward rotation reached on average 25° around ball release. The main motion is illustrated in Figure 4, which shows a stick diagram at five instances during motion with the scapula highlighted.

The high speed camera footage showed that the acromion cluster tilted forwards a bit relative to the acromion at that instance, due to its inertia. This is at the moment of the peak in forward rotation, which is illustrated by the red circle in Figure 5b.

Arm segment rotations can be estimated by using the thoracohumeral motion and using the motion of the scapula relative to the humerus. The mean maximum values for these two approaches of estimating arm segment rotations are shown in Table 4, as well as the difference between the mean maximum angles of the two approaches. The largest difference was found when horizontal abduction and adduction were compared, with an average of almost 50° of the maximum angles. This is because of the high scapular protraction that is reached, which was on average over 70°.

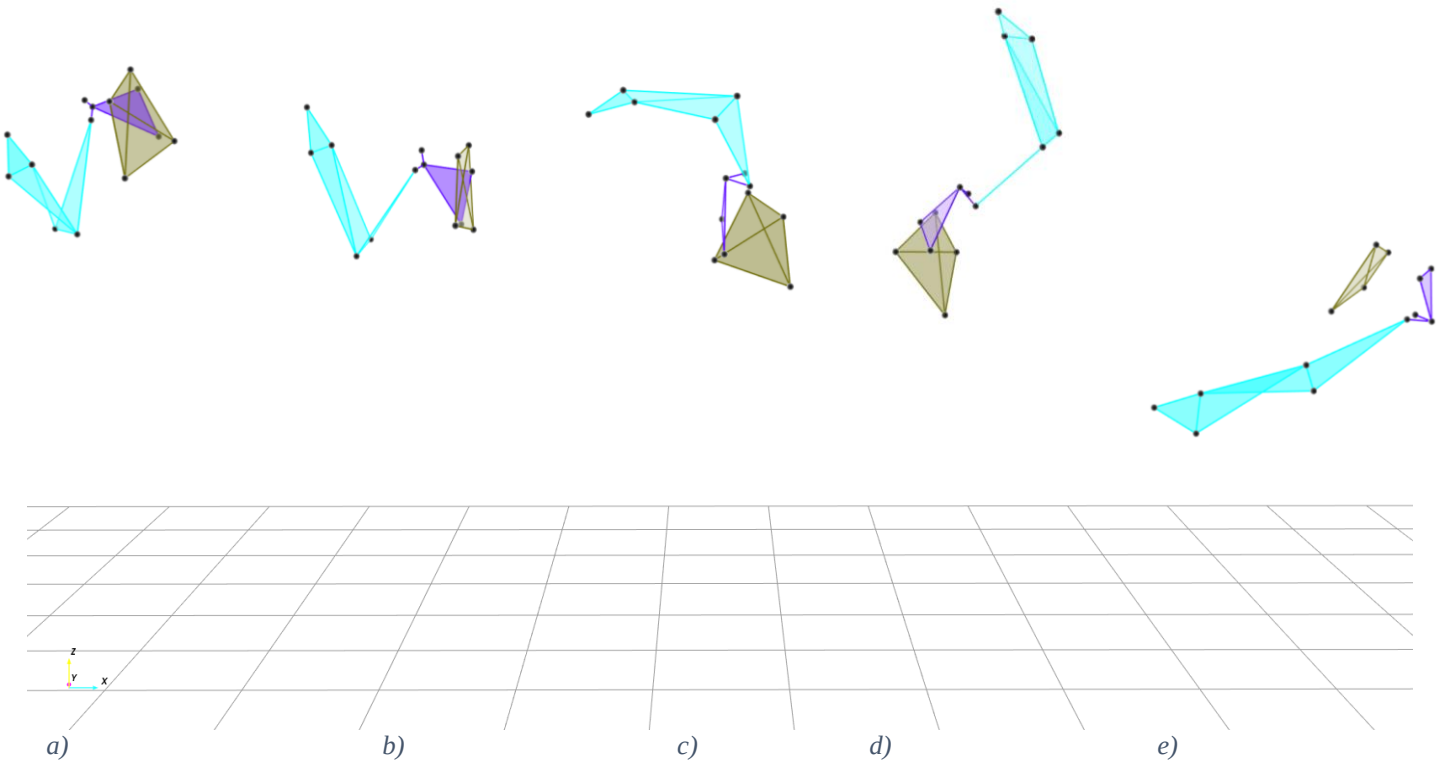

Figure 4: Stick diagram showing the thorax (green), scapula (purple), and arm (blue) for the windup (a), arm cocking (b), maximum external rotation (c), ball release (d) and follow-through (e).

Table 1: Pitching age, height and weight and their ball velocity (BV) in miles per hour and number of strikes (out of 5)

Subject #	Age	Height	Weight	BV range (mph)	BV mean (mph) ± SD	# of strikes
S1	15	184.0	76.4	77-78	77.6 ± 0.55	3
S2	16	188.5	80.9	60-75	68.2 ± 6.76	3
S3	16	197.4	90.0	69-75	73.4 ± 2.51	4
S4	16	185.0	87.7	81-81	81.0 ± 0.00	3
S5	15	186.0	64.8	75-78	76.6 ± 1.14	1
S6	17	188.5	70.9	72-74	72.8 ± 0.84	3
S7	16	185.8	74.5	75-78	77.0 ± 1.22	4
S8	15	183.0	61.4	71-73	72.0 ± 0.71	3
S9	16	182.4	93.8	73-75	74.0 ± 0.71	3
S10	16	191.5	69.0	71-74	73.0 ± 1.22	3
S11	15	182.2	73.6	74-77	75.4 ± 1.34	1
S12	17	176.8	71.7	73-74	73.8 ± 0.45	2
S13	17	188.5	72.5	70-73	72.0 ± 1.41	4
S14	16	186.7	76.2	74-75	74.8 ± 0.45	4
S15	17	174.0	75.0	76-78	77.4 ± 0.89	0
S16	16	187.7	79.8	70-72	71.0 ± 1.00	2
S17	15	184.0	76.0	77-80	78.2 ± 1.10	4
S18	15	169.0	51.0	67-69	67.8 ± 0.84	3
S19	16	203.0	83.0	71-74	72.4 ± 1.14	1

Table 2: Pearson correlation coefficients for relationships between maximum ball velocity and age, height and weight

Variable	Mean ± SD	r		r^2	P value
Age	15.9 ± 0.74 year	-0.133		0.018	0.588
Height	185 ± 7.6 cm	0.0504		0.003	0.838
Weight	75.2 ± 10 kg	0.410		0.168	0.081

Table 3: Mean maximum values of angles between scapula and thorax averaged over 5 pitches

Segments	Rotation	Mean (°) ± SD
Scapula relative to thorax	Retraction	6 ± 0.5
	Protraction	71 ± 3.1
	Lateral rotation	7 ± 1.2
	Medial rotation	28 ± 1.6
	Forward rotation	25 ± 0.9
	Backward rotation	17 ± 1.8

Table 4: Mean values of maximum segment angles over 5 pitches

Segments	Rotation	Mean (°) ± SD
Humerus relative to thorax	Horizontal abduction	53 ± 1.3
	Horizontal adduction	124 ±4.6
	Depression	27 ±1.5
	Elevation	114 ±1.7
	External rotation	167 ±1.4
	Internal rotation	23 ±2.5
Humerus relative to scapula	Horizontal abduction	53 ±1.0
	Horizontal adduction	74 ±6.3
	Depression	31 ±2.3
	Elevation	96 ±4.0
	External rotation	147 ±0.9
	Internal rotation	7 ±3.2
Difference	Horizontal abduction	1 ±0.8
	Horizontal adduction	50 ±2.4
	Depression	4 ±1.2
	Elevation	18 ±4.2
	External rotation	20 ±1.6
	Internal rotation	16 ±0.7

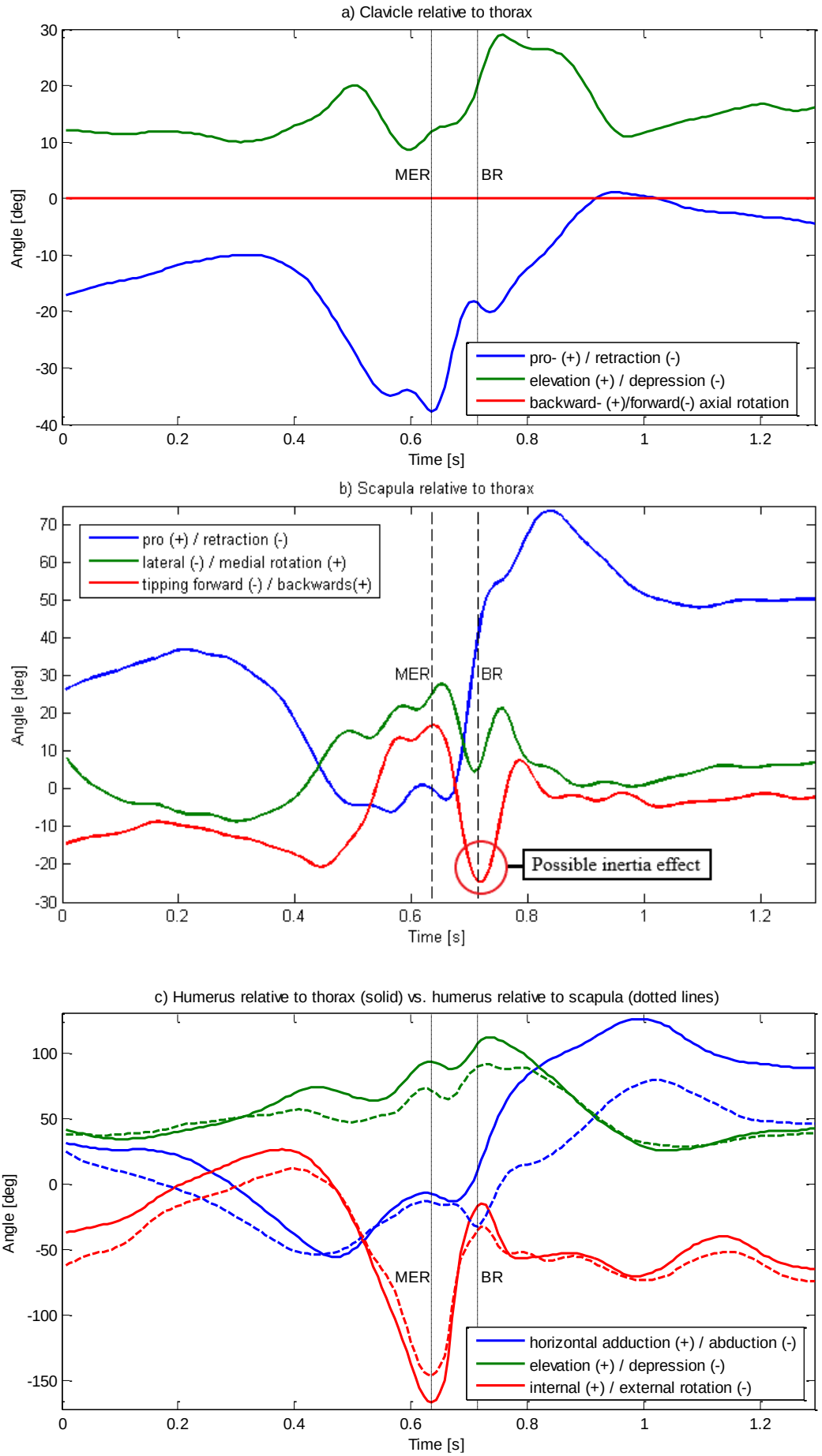

Figure 5: Bone rotations of a single pitch. MER: maximum external rotation. BR: ball release. '+' are positive values, '-' are negative values.

2.3.2 *Force measurements and scaling*

The average maximum force of the subjects was highest with pulling (260N ± 57) and lowest with external rotation (93N ± 26). Two subjects had a higher force upwards than with pulling, as shown in Table 5. For right handed subjects, internal rotation refers to left and external rotation refers to right. For left handed players, this was opposite. Two subjects (S1 and S5) produced more force upwards than with pulling.

The maximum force of the model was highest with pulling (265N) and lowest with both external rotation and upward rotation (125N). This is shown in the last column of Table 5. The scaling factors, shown in the last row of Table 5, ranged from 1.11 to 2.02. For all subjects, the direction that resulted in the scaling factor was 'up'.

2.4 DISCUSSION

2.4.1 *Kinematic measurements*

The pitching motion was recorded using an acromion cluster to track the scapula. A new design, using the same working principal as the designs of other acromion clusters found in the literature (Karduna et al., 2001, Meskers et al., 2007, van Andel et al., 2009), was used to make it suitable for the pitching motion. Validation of this specific design has not been performed yet, but this is in progress at the moment of writing. Previous studies using other acromion clusters reported to be accurate up to 120° of humeral elevation (Karduna et al., 2001, Meskers et al., 2007, Prinold et al., 2011). Humeral elevation is generally between 80° - 100° in pitching (Dillman et al., 1993, Myers et al., 2005, Downar and Sauers, 2005). For this subject, elevation of the humerus relative to the thorax was maximum 114° on average for the 5 throws, none of them exceeded 120°. Apart from inaccuracies for large humeral elevation, the orientation of the cluster during the motion is very sensitive to the attachment location (Shaheen et al., 2011). This is because the flat part of the acromion is larger than the base of the cluster, allowing for differences in attachment location. Additionally, this method allows for differences in the initial orientation of the cluster. Inconsistency of attachment location and orientation between and within operators will cause inaccuracies. The validation study that is in progress should quantify the possible inter- as well as intra-operator variability of the attachment location and initial orientation. Because of the lack of a validation study at this moment for this design, an attempt will be made to describe sources of inaccuracies.

Marker-based methods using non-rigid attachment to bony landmarks by definition involve significant inaccuracies, predominantly because of skin deformations (Cappozzo et al., 1997, Holden et al., 1997, Reinschmidt et al., 1997). In this study, the markers were attached to a tight shirt instead of directly to the skin, so shirt movement was actually the source of inaccuracies. The differences in inaccuracies between skin or shirt attachment have not been quantified, but are expected to be larger for the shirt, because a shirt can move more easily than skin, even if it's tight.

Since the cluster was taped to the shirt, lacking a rigid fixation to the acromion, the high accelerations in the pitching motion combined with the inertia of the acromion cluster could also cause rotations of the cluster relative to the acromion. After looking at the high speed camera footage, some effect of the inertia was found to be present just after ball release, which gives reason to believe that there is slight overestimation of the forward tilt of the scapula for a brief period. This was due to the inertia of the cluster at the moment of acromion deceleration. The consequences of this effect for modelling will be discussed in Chapter 3.

Another possible source of inaccuracies was the deltoid muscle pushing against the cluster. The deltoid contracts during humeral abduction and inevitably makes contact with the cluster. This effect is even larger when the subject is muscular, like many pitchers are in their upper extremities. The direction which the deltoid would push the cluster in depends on the position of the subject. At the end of the cocking phase the humerus is externally rotated and the anterior fibers of the deltoid contract. This would result in the deltoid tilting back the cluster and overestimation of backward rotation of the scapula. In the follow-through the humerus is internally rotated and the posterior fibers of the deltoid contract. This would result in the deltoid tilting forward the cluster and overestimation of the forward rotation of the scapula.

When using these kinematic data for simulation, it should be taken into account that the effect of all sources of inaccuracies are inevitably enlarged for this specific motion: pitching. Large bone rotations will increase the possible effect of the deltoid pushing against the cluster, and high velocities and accelerations increase the shirt motion and the inertia effect of the cluster. So, using the same measurement method, just because of the nature of the motion a measurement for pitching will be less accurate than one for a slow motion with small bone rotations.

Table 5: Maximum force [N] of the subjects in six directions. Internal means internal rotation, external means external rotation

Direction	S1	S2	S3	S4	S5	S6	S7	S8	S9	S10	S11	S12	S13	S14	S15	S16	S17	S18	S19	μ	σ	Model
Push	159	168	212	225	128	167	259	134	157	183	184	145	211	170	134	157	229	140	202	177	37	175
Pull	220	320	233	322	187	241	332	218	232	266	349	194	248	288	291	221	347	153	277	260	57	265
Internal	122	113	108	150	102	162	175	113	152	137	135	151	108	143	166	136	147	88	119	133	24	145
External	93	54	90	150	53	117	120	76	87	109	106	75	79	108	125	85	107	60	71	93	26	125
Up	252	167	177	220	196	192	251	199	182	211	198	183	203	245	234	200	222	139	176	203	30	125
Down	183	121	172	202	113	153	210	127	177	160	166	134	127	162	160	140	162	86	144	152	31	170
Scaling factor	2.02	1.34	1.42	1.76	1.57	1.54	2.01	1.59	1.46	1.69	1.59	1.46	1.62	1.96	1.87	1.6	1.78	1.11	1.40	1.60	0.20	

This dataset, obtained from the experimental study in Chapter 2, with angles for all joints of the shoulder region for one subject (S18) enables us to use a complete musculoskeletal model which contains all joints of the shoulder region, like the DSEM. This dataset will be used in the Chapter 3 in a simulation study. For simulation, the extreme character of the motion might cause problems. For the DSEM, validation was performed with simulations of rather slow movements, away from the limits of the range of motion of the shoulder joints (Nikooyan et al., 2010). In pitching however, there is high horizontal abduction and external rotation of the humerus. Besides, it was shown that there is a shift in range of motion of the glenohumeral joint on the throwing side for pitchers, where maximum external rotation increases and maximum internal rotation decreases (Brown et al., 1988, Ellenbecker et al., 2002). As a consequence, larger bone rotations will be used as a model input than the rotations in the validation study by Nikooyan et al. (2010). Range of motion has previously been measured for this subject group. It is recommended to apply the results of these measurements by judging if this change in range of motion on the throwing side is present. The difference in range of motion can cause incompatibilities between the subject and the model. More specifically, the bone rotations of the subject applied to the geometry of the model might not fit the kinematic constraints in the model. This will be described in Chapter 3. Additionally, large bone rotations increase the likelihood of muscle wrapping issues. Muscles in the DSEM are modelled as frictionless string-like objects. Generally a straight line from origin to insertion describes their line of action, however often muscles wrap around a bony contour. For instance, the serratus anterior wraps around the thorax, which is modelled as an ellipsoid (Van der Helm et al., 1992). Singularities can occur, meaning that there are multiple trajectories possible around the bony contour, which are the shortest. This can result in jumps in muscle lengths.

2.4.2 Force measurements and scaling

In contrast to MRI measurements, the force measurement that was performed was quick and could easily be implemented in a measurement protocol that also includes kinematic measurements of the pitching motion. Such a protocol can deliver a dataset aiming at using a musculoskeletal model. This protocol allows the maximum force of that model to be individually scaled for all subjects using a single factor. Because the scaling factor is the highest for upward force for all subjects, taking the maximum scaling factor over all directions actually meant using the scaling factor for upward force. This means that using this approach, only a force measurement using a single direction instead of six would be sufficient to find the scaling factor.

The position was assumed to be constant during the measurements, but was not recorded to allow the measurement to take place in a larger measurement protocol involving kinematic measurements of pitching without increasing protocol duration unacceptably. However, the maximum forces are sensitive to position changes, which follows from the force-length relationship of muscles.

The relationship of the maximum forces in the six directions was not consistent between the subjects and the model. Upwards was second, so relatively high, on average for the subjects, while it was lowest for the model. This means that beside differences in maximum force for all directions, which were expected because of strength differences, there were also large differences in normalized force over the six directions, which was more surprising. These differences in normalized force were also visible between the subjects: two subjects didn't exert their maximum force with pulling, like all others, but with upward force. In the results section (2.3.2), only the maximum value of the three trials was shown for all subjects, but the results of the other trials showed consistency for most subjects in the sense that they exerted their highest force in the same direction for all trials. This, however was not the case for S6, S10 and S18, whose direction of maximum force was not the same for all trials. Bolsterlee et al. (2015) found the maximum force to be the highest with pulling for 4 of the 5 subjects and with pushing for the other subject. So, both these maximum force measurements and the study by Bolsterlee et al. (2015) showed differences in the direction where subjects exerted their maximum force in. This suggests that there are actually large differences in normalized force between people. This could also explain that the normalized maximum muscle force in the six directions differs from the model to the subjects.

The choice has been made to deliver individualized scaling factors. Instead, the mean or maximum scaling factor of all subjects could be used to scale PCSA for all subjects. However, because the large differences in maximum force between the subjects, resulting in a range of scaling factors from 1.11 to 2.02, taking the mean value of 1.60 would result in the force in the model being too limited for the strongest subjects. When taking the maximum scaling factor of 2.02, all subjects should have enough force in the model, but some subjects would have a higher muscle force in the model than in reality. This doesn't necessarily impede proper simulation, but was not done because realistic scaling factors were preferred. However, the disadvantage of this is that all kinematic measurements should be performed along with maximum force measurements.

Instead of using an individualized scaling factor, another option would be to use a single factor for PCSA scaling for all subjects. Bolsterlee et al. (2015) found that the effect of PCSA scaling during simulation of humeral elevation was mainly increasing maximum strength, but there was little effect for tasks with submaximal force. This means that having too much force would have little effect. So, when no individual scaling factor is available, it is recommended to use the maximum scaling factor found.

The effect of scaling PCSA should be investigated by a simulation study, which will be done in Chapter 3. This chapter will also be an attempt in simulating the obtained pitching kinematics in the DSEM.

3 Simulating the pitching motion in a musculoskeletal model of the shoulder region

A case study

3.1 INTRODUCTION

In Chapter 2 a dataset was obtained consisting of upper limb kinematics of the pitching motion and a PCSA scaling factor, which can be used as an input for a musculoskeletal model. There have not yet been any reports on simulations of the pitching motion in a musculoskeletal model of the shoulder region. This chapter will describe a study where this kinematic dataset is used as an input for the DSEM, with the goal of performing a complete simulation. Also, the influence of PCSA scaling will be investigated. To be able to report results of different parts of the model, it is required to describe the model's structure first.

When using a motion as input to estimate muscle force, the inverse-dynamics mode of the model can be used. The inverse-dynamics mode basically consists of two parts: a kinematic model (inverse skeleton dynamics) and a dynamic model (muscle force-length relationship and muscle load sharing), as illustrated in Figure 6. The force-velocity and passive force-length relationship are not included in the inverse–dynamics model of the DSEM, but they are in the inverse-forward-dynamics optimization with controller model of the DSEM (Nikooyan et al., 2011).

The kinematic model calculates for each time step the acceleration around the joint from the joint angles. The joint moments are then calculated from this acceleration, and the segment mass using inverse skeleton dynamics. It also calculates the muscle lengths in each time step from the joint rotations. Compared to a model of the lower limb, which is an open-loop system, shoulder modelling faces additional challenges because the shoulder region is a closed-loop mechanism. That means that, because of differences in dimensions of bones, some rotations of the subject are not possible for the model. For this reason, optimization of the input angles is required to make the input angles compatible with the model. This takes place in the kinematic model as well, which optimizes the input angles for the clavicle relative to the thorax and the scapula relative to the thorax at the beginning of simulation. This optimization takes place by fulfilling two constraints of the closed-chain mechanism, while minimizing differences to the input angles ($\bar{\theta}_{meas}$). The motion of the scapula is constrained to be on a fixed distance to the thorax, which is modelled as an ellipsoid. To be more precise, the distances of both the trigonum spinae (TS) and angulus inferior (AI) are constrained. Also, the length of the conoid ligament, which connects the scapula to the clavicle, is constrained to be constant. Because no movement or length change is allowed, this is called a hard constraint, which is used by default in the DSEM. Instead of a hard constraint, a soft constraint could be used for the angle optimization, allowing some variation in distance from scapula to thorax and conoid length. When using the soft constraint, the optimized angles ($\bar{\theta}_{sim}$) are calculated by minimizing the sum of J_θ and J_{con} weighted by 'wf' as follows:

$$\min(J_\theta + wf * J_{con})$$

Here J_θ is defined as the summed squared difference between $\bar{\theta}_{sim}$and $\bar{\theta}_{meas}$:

$$J_\theta = \sum_{i=1}^{6} \left(\bar{\theta}_{sim}(i) - \bar{\theta}_{meas}(i)\right)^2$$

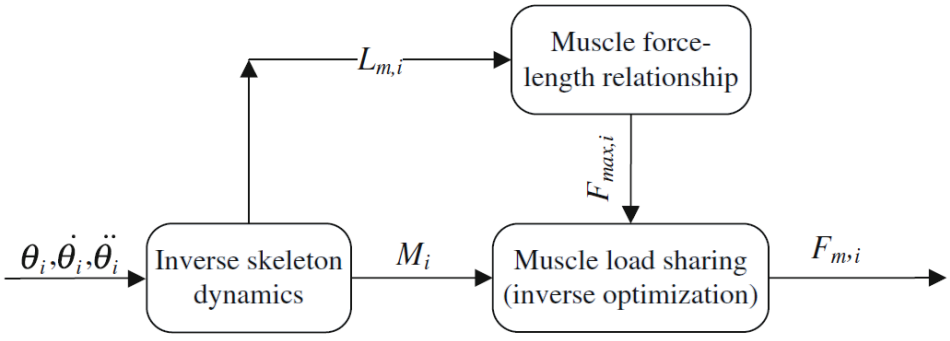

Figure 6: Inverse-dynamics model structure of a musculoskeletal model with the following parameters: joint orientation (θ), velocity ($\dot{\theta}$), acceleration ($\ddot{\theta}$), muscle length (L_m), joint moments (M), maximum muscle force (F_{max}) and muscle force (F_m) at each time sample (i) (Nikooyan et al., 2011).

where i is the number of the orientation angle J_{con} is defined as the square of the deviation from the three constraints summed:

$$J_{con} = (dTS_{sim} - dTS_0)^2 + (dAI_{sim} - dAI_0)^2 + \left(l_{con,sim} - l_{con,0}\right)^2$$

With dTS_{sim} the distance of TS to the thorax, dAI_{sim} the distance of AI to the thorax, and $l_{con,sim}$ the conoid length (Bolsterlee et al., 2014). An infinite weight factor would result in optimized angles equal to those from the hard constraint. A weight factor of zero would result in optimized angles equal to the input angles. The input angles might be incompatible with the model, but most accurately describe the actually performed motion. When using the hard constraint the optimized angles might have large differences with the input angles, but will fit the model motion options perfectly. A weight factor in between zero and infinite can be used to find a compromise between using the input angles and the optimized angles when using the hard constraint. Bolsterlee et al. (2014) used the soft constraint with a weight factor of 0.01, because this resulted in a satisfactory compromise for simulation of a humeral elevation task.

After having described the kinematic model, a judgement can be made on the significance of the two possible problems found with the kinematic data in Chapter 2: first, not having measured clavicle axial rotation, and second, the possible overestimation of the scapula forward tilt because of the inertia of the acromion cluster. Both of these rotations can be optimized to be compatible with the geometry of the model. However, not just fulfilling the model constraints is desired, but also optimized angles that have small differences to the input angles. Running the kinematic model can give insight in the ability of the model to optimize the input angles of the clavicle and scapula and it also shows how the muscle lengths change over time.

The dynamic model estimates the muscle forces through optimization using an energy-based load sharing criterion (Praagman et al., 2006, Nikooyan et al., 2011). This is required because there are more muscles than degrees-of-freedom in the model, in other words there is an infinite number of solutions at each time step. The estimated muscle forces are independent of the previous time samples (hence the often used term 'static optimization') and are restricted by a maximum muscle force that depends on muscle geometry and physiological parameters. The maximum force is also restricted by the relative force available at the current length, calculated from the active force-length relationship. The consequence of maximum force being limited by the force-length relationship is that when muscles reach very low or high lengths, they will hardly be able to produce any force, or no force at all. In the latter case, PCSA scaling will have no effect.

Running the dynamic model can give insight in its ability to solve the muscle force optimization, in other words if the model is able to find a combination of muscles that can generate enough force to generate the high segment acceleration that occur in the pitching motion. If the required force is too high, or the available force is too low due to extreme muscle lengths that occur near the end of the range of motion, the model will not be able to find a solution in the muscle force optimization routine.

3.2 METHODS

A kinematic recording of unilateral upper limb bone angles during the pitching motion of a 15 year old AAA level pitcher (height 169 cm, weight 51 kg, S18 from Chapter 2), consisting of 200 frames sampled at 140 Hz, was used as an input for the DSEM (version 4.2 in Matlab 2014a, Mathworks).

First, the input was used for the kinematic model, to isolate the performance of this part of the model. The optimized angles of the clavicle relative to the thorax and the scapula relative to the thorax were compared to the input angles by calculating peak differences between the rotations and root mean square (RMS) of the difference of the rotations. The relative muscle length was compared to the active force-length relationship to quantify to what extent the muscles were at a length that allowed them to generate a significant amount of force. Changing input angles of the clavicle axial rotation and the scapula forward rotation, as well as different optimization routines were used to study their effect on the processed angles. These different optimization routines were using different combinations of weight factors for the input rotations as well as using a soft constraint, as described by Bolsterlee et al. (2014), instead of a hard constraint. For the soft constraint, weight factors of 0.01 and 0.2 were used. This was done because the weight factor of 0.01 was used by Bolsterlee et al. (2014), and the weight factor of 0.2 resulted in a better compromise between using the input angles and the optimized angles when using the hard constraint. The equations that describe the meaning of this weight factor are shown in 3.1.

Finally, the input was used for the complete version of the DSEM, including both the kinematic and dynamic model, to investigate the model's ability to find a solution of the muscle force optimization in each time step. The effect of PCSA scaling was found by running the same input file in the DSEM with the following scaling factors: 1, 1.25, 1.5, 1.75, 2, 3, 5 and 10. Then the number of frames was counted where muscle optimization found a solution. The model was adapted with different force-length curves to investigate the influence of relative muscle length on muscle optimization. This was done using the hard constraint, as well as the soft constraints with weight factor 0.01 and 0.2.

In all simulations, the rotations of the thorax were set to zero, because the relatively large thorax rotations cause problems in the first kinematic step of the model. This is an issue that was already known to the research group.

3.3 RESULTS

3.3.1 Running the kinematic model of the DSEM

The pitching kinematic input file of one subject measured with the acromion cluster consists of 200 frames (140 Hz). The kinematic model didn't find a solution in the 89th step in the kinematics, exactly the moment of maximum external rotation of the humerus. This was because the scapula was reported to be inside the thorax.

There were big differences between the input angles and the optimized angles, as can be seen in Figure 7. Most striking were the jumps that are visible from the 72nd to the 73rd frame and from the 87th to the 88th frame, where the angles are again close to where they were at the 72nd frame. The resulting motion from the optimization clearly contained artifacts and didn't represent a realistic motion. The consequence of the jumps in the clavicle and scapula rotations are directly visible when looking at muscle length. These jumps caused a sudden length change, which can be seen when looking at the 12 muscle elements of the serratus anterior, which is a muscle attached to the scapula, in Figure 8. This figure shows that the jumps in the optimized angles can cause jumps both up and down in length within a single muscle.

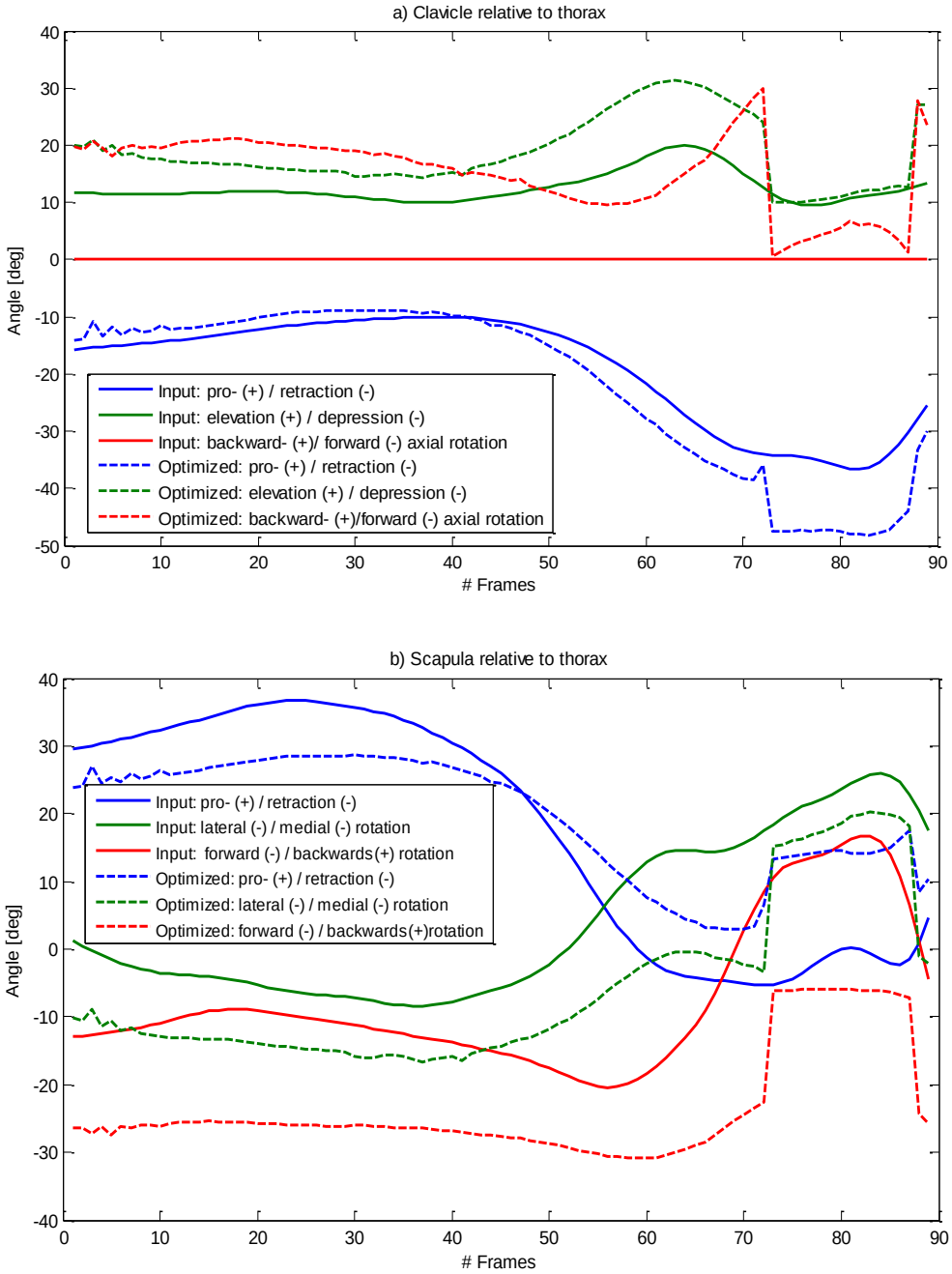

Figure 7: Comparison between input and optimized angles for the clavicle (a) and scapula (b) relative to the thorax. '+' are positive values, '-' are negative values.

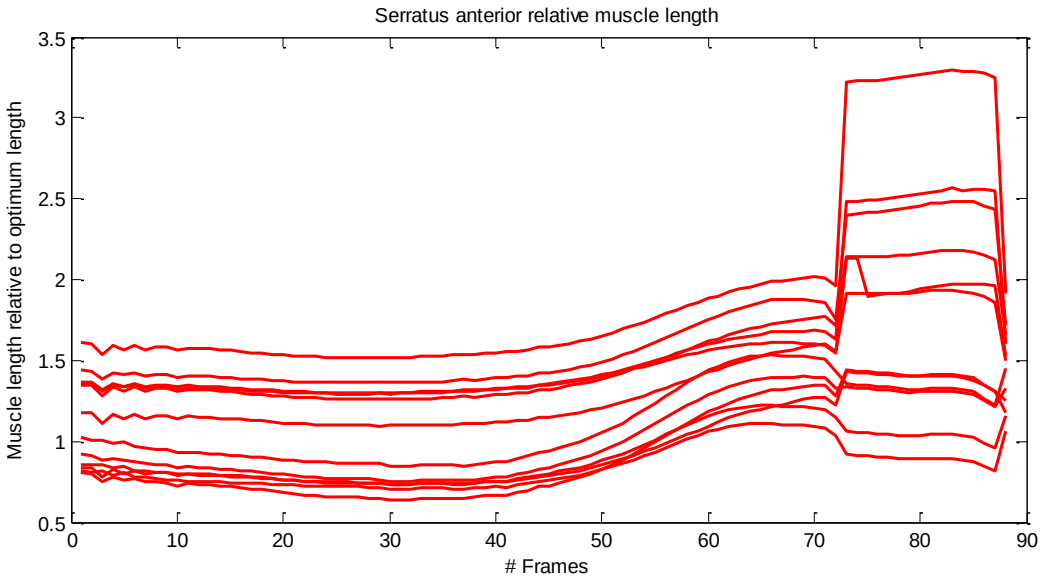

Figure 8: Muscle length of the 12 muscle elements of serratus anterior

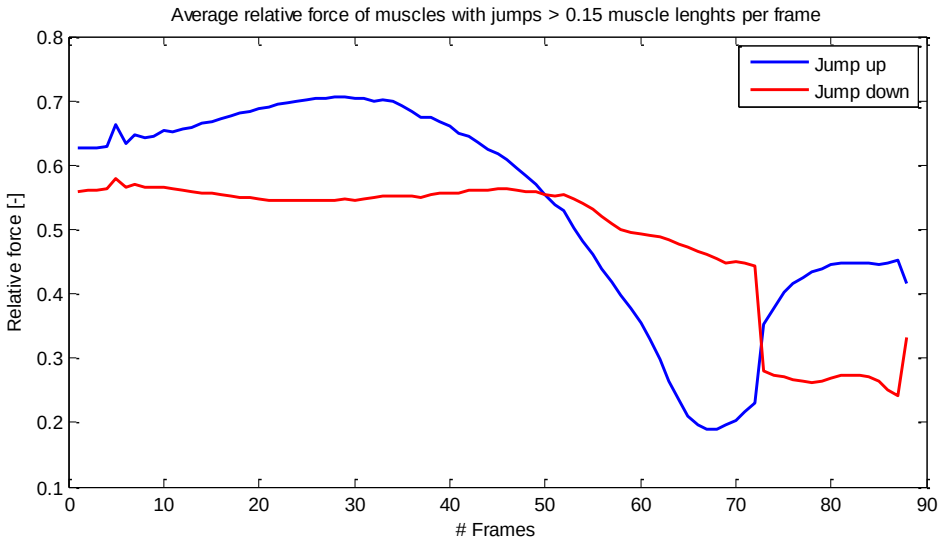

Figure 9: Relative force averaged over all muscle elements with jumps > 0.15 muscle lenghts per frame

The fact that the model didn't find a solution for the joint angle optimization in the 89th step is surprising, because the angles used in simulation are optimized to fit to the constraints and therefore are assumed to be already compatible with the model. It is difficult to find the cause of this, as it is not possible to isolate the problematic frame, as the optimization of the angles takes the previous frame into account. As mentioned earlier, besides fulfilling the constraints, the optimization tries to minimize the difference with the previous frame. This is illustrated by an additional simulation performed starting with the 89th frame. This simulation finds solutions for frames 89 to 132. So, the problems for frame 89 are also caused by frame 88, which also depends on the frame before that and so on.

The high jumps in the optimized angles are not problematic solely because of the fact that it doesn't represent the actual motion, but more directly because it causes high jumps in muscle length, often to lengths far from the optimum length. From the active force-length relationship it is known that muscles with lengths far from the optimum length will not be able to generate a significant amount of force at these points, making it less likely that a solution will be found in the muscle force optimization routine of the dynamic model. 41 of 139 muscle elements showed large jumps in length (> 0.15 muscle length/frame), 18 of them jump up, 23 down. The effect of these jumps on the maximum relative force is shown in Figure 9, showing the average of the elements that jump up and the ones that jump down respectively. The muscle elements that jump down are below 30% of their maximum relative force during this jump.

To solve the problems that arise during the angle optimization, there are two ways to influence the optimized angles: by changing the input kinematics and by changing the optimization routine.

3.3.2 Changing input kinematics

Generally, it would be undesirable to change the input kinematics, because this would mean that the motion that is used as the input would not be the same as the motion that was recorded. However, exceptions for this specific case are the clavicle axial rotation and the scapula forward rotation: the clavicle axial rotation was not measured and was set to zero for the complete motion in the input kinematics, under the assumption that the optimization of the input angles would find reasonable angles for the axial rotation. However, besides fulfilling the constraints, this routine is still trying to minimize the differences to the input angles. It could help to use a rough estimation of the clavicle axial rotation as an input, which will then be optimized in order for the model not to minimize the differences with zero axial rotation. An attempt to this was made by using downscaled rotation of the scapula rotating forward and backward for the axial rotation of the clavicle, based on the assumption that these rotations are related. The rotations are downscaled due to the assumption that the scapula rotating forward requires a forward axial rotation of the clavicle of a smaller angle. Scaling factors between 0 and 1 in increments of 0.1 were used. Also, the possible overestimation of scapula rotating forward after ball release was a reason to downscale the peak again with scaling factors between 0 and 1 with increments of 0.1. Scaling of this peak was combined with using the scapula rotating forward and backward angles for the clavicle axial rotation with different scaling factors, resulting in a total of 100 simulations. The effect was found by comparing maximum differences between input angles and output angles and by comparing maximum differences in angle between adjacent frames, which is a measure for how big the jumps are.

Both of these measures were very high for the original input kinematics and changing the input kinematics didn't result in significantly lower values for both measures, but more often resulted in much higher values.

3.3.3 Changing angle optimization routine

Another option to influence the optimized angles is to change the angle optimization routine. This can be done in two ways: by changing the weight factors of the six angles and by changing the constraints.

3.3.3.1 Changing weight factors

As mentioned before, apart from just fulfilling the constraints, the optimization tries to minimize the difference with the input angles. Different weight factors are used for different rotations to show which rotations should be the most relied upon. The default weight factors for the six rotations are shown in Table 6. As mentioned in 2.4.1, the clavicle axial rotation that was not measured and was set to zero in the input kinematics still has a weight on it causing the model to try to minimize differences with zero axial rotation. Lowering the weight will reduce this, although having no weight at all on it may increase the probability that unrealistic rotations, such as very high clavicle axial rotation or large jumps, will occur. Apart from the clavicle axial rotation, the combination of weight factors for all rotations might not be optimal for the input kinematics of this case. So, for all six rotations weight factors from 0-3 in increments of 1 and their combinations were used for the optimization routine. This resulted in 4^6 equals 4096 simulations. Again, the effect was found by comparing maximum differences between input angles and output angles and by comparing maximum differences in angle between adjacent frames. Changing the weight factors didn't result in significantly lower values for both measures, but more often resulted in much higher values.

3.3.3.2 Using the soft constraint

Using the soft constraint with weight factor 0.01, the kinematic model was able to find a solution for all frames. This soft constraint resulted in angles much closer to the input angles than with the hard constraint and with smaller jumps. However, the soft constraint with weight factor 0.01 caused high variation in the distances from TA (1.8 – 7.6 cm) and AI (0.5 – 4.3 cm) to the thorax as well as in conoid length (0.7 – 2.4 cm), as shown in Table 7. All these distances were constant using the hard constraint. To find a better compromise between fulfilling the constraints and staying close to the input angles, a soft constraint with weight factor 0.2 was used. Again, a solution was found for all frames as well as angles closer to the input angles, which can be seen in Figure 10. Small jumps occurred from frame 50 to 51 and back from 55 to 56. There was less variation in the distances from TA (3.3 – 4.2 cm) and AI (2.4 – 2.9 cm) to the thorax as well as in conoid length (1.4 – 2.2 cm), as shown in Table 8. However, differences with the input angle increased with changing the weight factor to 0.2. The RMS for the difference between input and optimized angles ranged from 4.3 – 8.7 for weight factor 0.2 and from 0.7 – 5.1 for weight factor 0.01. In addition, the highest difference between input and optimized angles increased from 12.3° to 21.1° after changing the weight factor from 0.01 to 0.2. To see this in perspective, using the hard constraint, the RMS ranged from 6.0 – 16.6 and the maximum difference was 129.1°. Using no constraints, both the TS and AI reached negative distances to the thorax, meaning the scapula going inside the thorax. Extreme length differences of 0.3 – 4.0 cm occurred for the conoid ligament.

Table 6: Default weight factors for the six rotations in the optimization of the angles

Segments	Rotation	Weight
Clavicle relative to thorax	Pro-/retraction	3
	Elevation/depression	3
	Backward-/forward axial rotation	1
Scapula relative to thorax	Pro-/retraction	2
	Lateral- medial rotation	3
	Rotating forwards/backwards	2

Table 7: Influence of constraint type on ranges of distance of TS and AI to thorax and conoid length. 'wf' means weight factor.

Constraint	TS distance (cm)	AI distance (cm)	Conoid length (cm)
Hard	3.7 – 3.7	2.6 – 2.6	1.9 – 1.9
Soft (wf = 0.2)	3.3 – 4.2	2.4 – 2.9	1.4 – 2.2
Soft (wf = 0.01)	1.8 – 7.6	0.5 – 4.3	0.7 – 2.4
None	-3.4 – 9.6	-6.0 – 5.2	0.3 – 4.0

Table 8: Maximum difference and RMS of input versus optimized angles

		Hard constraint		Soft constraint (wf = 0.2)		Soft constraint (wf = 0.01)	
Segments	Rotation	Max difference	RMS	Max difference	RMS	Max difference	RMS
Clavicle relative to thorax	Pro-/retraction	128.9°	6.0	12.7°	5.3	6.5°	3.1
	Elevation/depression	15.4°	7.1	9.3°	4.9	4.5°	1.5
	Backward-/forward axial rotation	129.1°	16.6	8.7°	4.3	1.7°	0.7
Scapula relative to thorax	Pro-/retraction	124.5°	9.2	21.1°	8.7	12.3°	5.1
	Lateral-/medial rotation	17.9°	10.4	13.9	6.3	5.4°	2.2
	Rotating forwards/backwards	31.7°	16.5	16.0°	5.9	8.4°	3.0

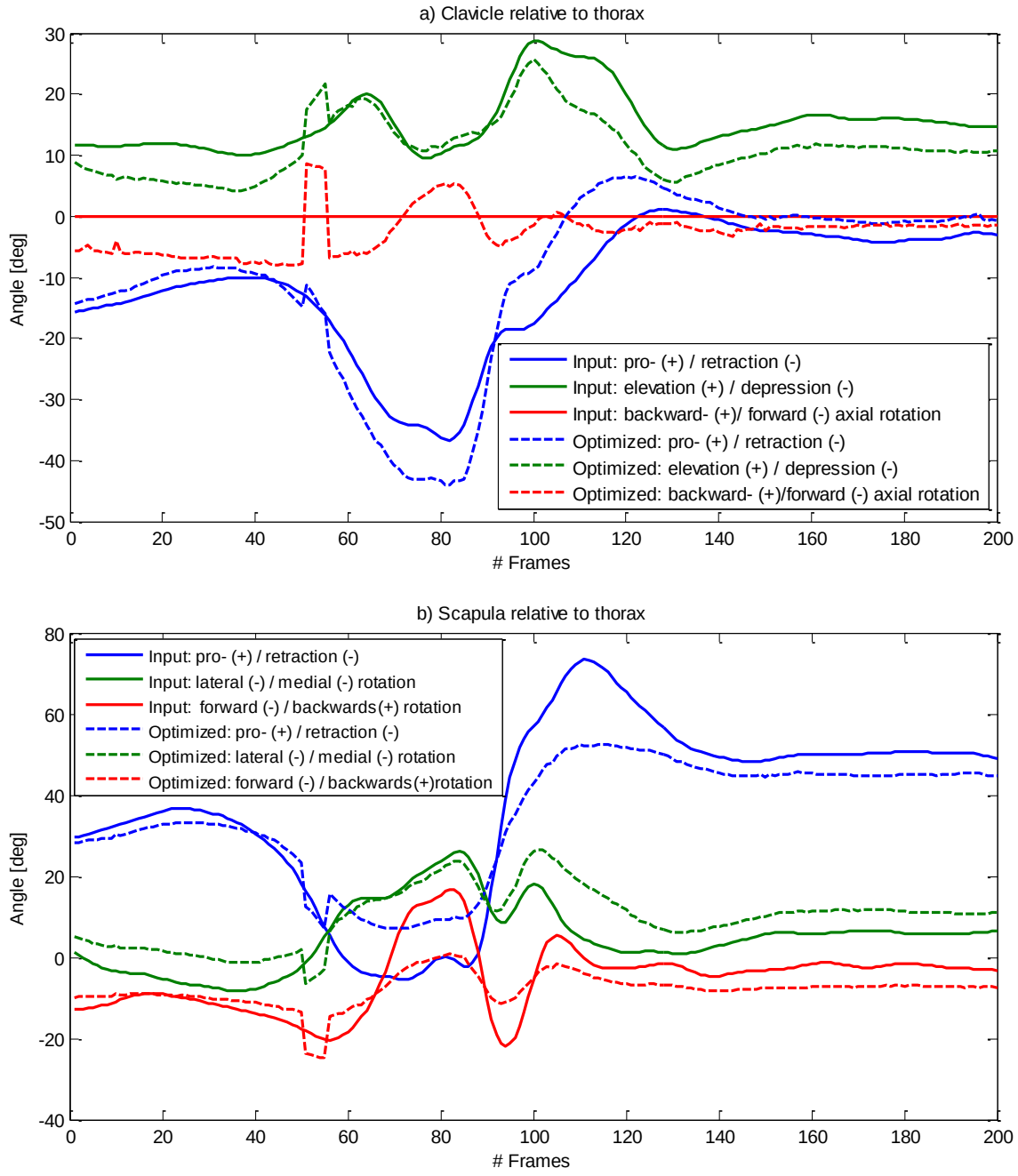

Figure 10: Comparison between input and optimized angles for the soft constraint with weight factor 0.2 for the clavicle (a) and scapula (b) relative to the thorax. '+' are positive values, '-' are negative values.

3.3.4 Running the dynamic model of the DSEM

When running the input with the hard constraint in the DSEM with the dynamic model, for only 21 out of 88 frames a solution was found in the muscle optimization. This number increased when upscaling PCSA, as can be seen in Table 9. Increasing PCSA with a factor of 3, 72 frames were solved, but with higher factors the number of frames hardly increased anymore (73 frames for a factor of 10). The frames that are not solved even with a very high PCSA scaling factor are 74 to 88, which are the frames that correspond to the period of jumps in the optimized angles. The fact that there are still frames not solved in the muscle optimization despite PCSA scaling is caused by the muscle lengths being far from the optimum length, partly because of the jumps in muscle length. The fact that these high relative muscle lengths are responsible for not finding a solution is illustrated by the following simulation: the active force-length relationship in the model was removed, which was achieved by setting the maximum relative force to 1 for all relative muscle lengths. Then, when running the model without PCSA scaling, 86 of the 88 frames were solved. The unsolved frames were in the acceleration phase. The jumps in optimized angles are not correct, so the effect of PCSA scaling can be seen more easily when using the soft constraints with reduced jumps. Because the large jumps in muscle length are not correct, it makes more sense to analyze the effect of PCSA scaling using the soft constraints, where there are still jumps, but only much smaller.

With the soft constraints, the number of frames solved in the dynamic model was a lot higher: without PCSA scaling the number of frames solved was 121 and 124 of the 200 frames for weight factor 0.2 and 0.01 respectively. This increased to 192 and 194 with a PCSA scaling factor of 10, as shown in Table 9. Removing the force-length relationship without PCSA scaling increased the number of frames solved to 172 and 168 for the weight factor of 0.2 and 0.01 respectively. The unsolved frames for both soft constraints after removing the force-length relationship were all in the acceleration phase.

3.4 DISCUSSION

The simulations done using the kinematic as well as the dynamic model have given a lot of information. The kinematic model using the hard constraint causes large jumps in the optimized angles and no solution was found at the 89th frame of the 200 frames. The solution was not found because the scapula was reported to be inside the thorax. This is odd, since the angle optimization with the hard constraint was designed to prevent this by means of keeping the scapula to a constant distance outside of the thorax. It is recommended to investigate this problem further by analyzing the input and the output during the simulation of all frames of the function that causes this error.

The jumps and the large differences in input angles and the optimized angles mean that the angles used in the simulation differ a lot from the measured angles, which is undesirable because it undermines the validity of the simulations. The jumps also cause problems for the dynamic model, because muscle elements jump to lengths far from their optimum, causing the force they're able to produce to be limited greatly because of the length dependency of muscle force.

PCSA scaling increased the number of frames that were solved in the muscle force optimization. However, much higher scaling factors than recommended in Chapter 2 (S18 corresponded to a factor of 1.11) were needed for large increases of number of frames solved, but still not all frames were solved.

Removing the length dependency of the maximum force was more effective than increasing PCSA using the hard constraint, because when a muscle is very far from its optimum length, increasing PCSA will still leave the muscle unable to produce a significant amount of force. Obviously, removing the force-length dependency is not recommended, this was merely done to pinpoint the problems. A relationship was found between unsolved frames in the muscle force optimization and jumps in the optimized angles, meaning that the insufficiency of muscle force despite scaling is at least partly caused by differences between input and optimized angles.

Table 9: Relationship between PCSA scaling factor and number of frames solved in the dynamic model

PCSA scaling factor	F-l relation-ship	Hard constraint	Soft constraint (wf 0.2)	Soft constraint (wf 0.01)
1	Yes	21*	121†	124†
1.25	Yes	26*	130†	126†
1.5	Yes	34*	144†	127†
1.75	Yes	43*	147†	132†
2	Yes	50*	154†	138†
3	Yes	72*	166†	161†
5	Yes	73*	185†	185†
10	Yes	73*	192†	194†
1	No	86*	172†	168†

*: number of frames solved of total of 88 frames
†: number of frames solved of total of 200 frames

The fact that even extreme PCSA scaling resulted in unsolved frames by the dynamic model, might be caused by differences in musculoskeletal properties. For the humerus, maximum external rotation is increased and maximum internal rotation is decreased (Brown et al., 1988, Ellenbecker et al., 2002). This implies that pitchers may have a larger optimum muscle length or a shifted working range. If that would be the case, the active force-length relationship in the model would drastically limit muscle force at lengths that are modelled to be way above or below optimum length, but in reality might be much closer to the optimum length. It is recommended to investigate if there's a difference in optimum muscle length for pitchers and to scale this in the model if that would be the case. This could have drastic effect on how many frames are solved by the dynamic model.

Changing the weight factor of the clavicle and scapula rotations relative to the thorax and changing the input kinematics didn't improve the optimized angles in the sense that there were still high jumps and angles far from the input angles in the processed angles. However, using soft constraint did have major impact. Optimized angles were much closer to the input angles and only small jumps were visible. The kinematic model found solutions for all frames.

As a recommendation for future research that will have to deal with the modelling challenges laid out here, it is important to conclude that the key problem is the optimization of the clavicle and scapula angles relative to the thorax. The fact that the optimization causes issues with the pitching data, but not with other motions (Nikooyan et al., 2010), is likely because the motion is more extreme. The extreme character of the pitching motion, described by large bone rotations, velocities and accelerations, is accompanied with decreased measurement accuracies, as described in 2.3.1. Besides possible inaccuracies, the large bone rotations itself can increase the difficulty of angle optimization.

Using the hard constraint might be realistic in an ideal situation, but is in many cases problematic. Incompatibilities between model and subject geometry arise from measurement inaccuracies and by the fact that there is large inter-individual variance in scapula geometry (Wolffson, 1950, Krobot et al., 2009) and conoid length (Harris et al., 2001, Takase, 2010). Individualization by means of segment scaling can compensate for this, but will increase the difficulty of fulfilling the hard constraint in the model (Blemker et al., 2007, Prinold et al., 2013). This hard constraint, representing the fact that all the joints in the shoulder are linked, might be in accordance with actual shoulder functioning, but might be a problem when there are significant differences in geometry between subject and model and when measurements inherently are associated with a certain degree of inaccuracy. Bolsterlee et al. (2014) also proposed segment scaling of the model to fit the subject, which should be executed along with using the soft constraint. Segment scaling proposals are described by Prinold and Bull (2014). Bolsterlee et al. (2014) only used one soft constraint, in this study two were used. It is recommended to try even more, to find a good compromise between the angles being close to the measured angles and being compatible with the model.

The kinematic problems should be solved before being able to fully assess the effectivity of the use of PCSA scaling. This is due to the fact that the muscle lengths that are a consequence of kinematics that differ a lot from the measured kinematics limit the maximum muscle force greatly because of the length dependency of muscle force.

4 Muscle length and velocity during baseball pitching

A motion study

4.1 INTRODUCTION

Musculoskeletal modelling can give valuable information about the pitching motion. In the acceleration phase of the pitching motion, a lot of power is produced and a high humeral internal rotation velocity of sometimes over 9000°/sec is reached (Pappas et al., 1985, Fleisig et al., 1999). In Chapter 2 of this study a maximum internal rotation velocity of the humerus was found to be on average 5330 °/s ± 114 (one subject, five pitches). Knowing how exactly this high velocity is achieved could help to give insight into the motion, which then could open up possibilities to throw even faster and reduce injury rates.

An option to get information on the contribution of individual muscles is to use a kinematic model, which is able to estimate muscle length and velocity during the pitching motion. This information is valuable, because muscle force has been shown to be length and velocity dependent. The active force-length relationship has been implemented in the inverse-dynamic model of the DSEM. The force-velocity and the passive force-length relationship are not implemented in the inverse-dynamics model, but they are in the inverse-forward-dynamic optimization with controller model (Nikooyan et al., 2011).

Force-velocity curves for muscles are generally described by a hyperbolic function (Hill, 1938), as shown in Figure 11. An important parameter in this relationship is the intersection with the horizontal axis, V_0. This is the lowest velocity where no force can be exerted by the muscle. If the muscle contraction velocity of the muscles gets close to or beyond V_0, this would mean that these muscles are not responsible for the segment acceleration in the acceleration phase. An overview of values found in the literature for V_0, described as maximum unloaded shortening velocity, is given in Table 10.

The force-length relationship is shown in Figure 12. The peaks in the middle represent peak active force at optimum fiber

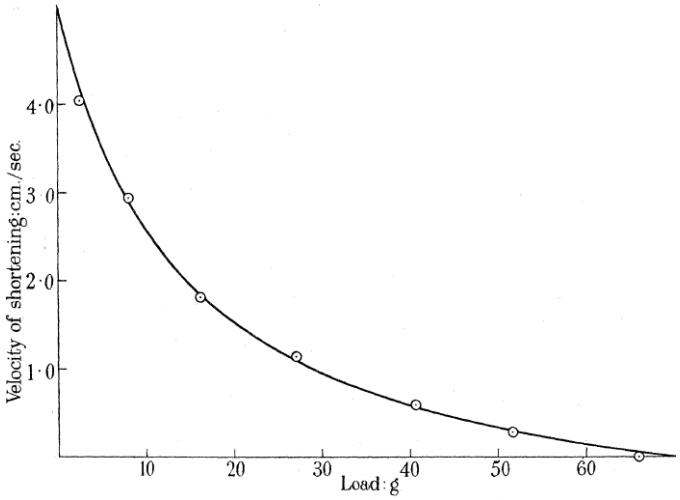

Figure 11: Force-velocity relationship as described by (Hill, 1938)

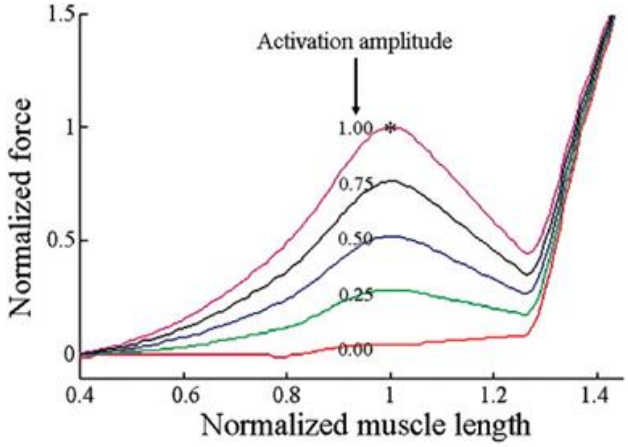

Figure 12: Force-length relationship (Yekutieli et al., 2005)

Table 10: Maximum unloaded shortening velocities (V_0)

Study	Species	Muscle	in vivo/vitro	n	range V_0 (ML/s)	mean V_0 (ML/s)
Morris et al. (2001)	Human	Masseter	in vitro	26	0.027-1.82	0.590 ± 0.511
		Leg (various)		18	0.125-1.141	-
Sasaki and Ishii (2005)	Human	Triceps surae	in vivo	10	0.5-3.4	-
Sasaki and Ishii (2010)	Human	Tibialis anterior	in vivo	6	4.2-9.9	-
		Soleus		6	-	7.02
		Extensor digitorum longus		6	-	13
Edman (1979)	Frog	Semitendinosus/ tibialis anterior	in vitro	25	-	2.7
Larsson and Moss (1993)	Human	Quadriceps	in vitro	86	0.2-4.1	-
		Soleus		17	0.2-1.0	-

length. The sudden increase in normalized muscle force after the peak doesn't represent active muscle force, but is the consequence of elastic forces. Elastic forces might play a role in the pitching motion by contributing to the acceleration, because it could be stored in the cocking phase and released in the acceleration phase.

A force transfer could be achieved with spring-like behavior. In the cocking phase, there is likely stretching of the muscle-tendon-units of the muscles that contract in the acceleration phase. These are those of the humeral internal rotator, adductor and scapular protractor muscles. The stretching of these muscle-tendon-units requires energy. This energy is provided in the cocking phase by either active stretching, caused by the opposing muscles, or because of inertia after trunk rotation. In the acceleration phase, this energy would then be released: the shortening of the structures results in elastic forces that contribute to the acceleration.

In this research, the pitching motion will be simulated in a musculoskeletal model of the shoulder region to obtain the muscle length over time, which relates to the elastic forces. The muscle length will then be used to calculate the velocity of the muscles, which relates to the amount of force the muscle is able to produce actively. A high shortening velocity would mean that the muscle will be unable to exert the force generating the motion. Chapter 3 showed that the recorded upper limb kinematics could be simulated completely with only the soft constraint, and could only partially be simulate with the hard constraint. This study will use another dataset which can be used for a complete simulation with the hard constraint. The optimized angles for this dataset were also closer to the input angles than with the dataset in Chapter 3 using either of the two soft constraints.

4.2 METHODS

Kinematic recordings of six pitches from four different subjects were used as an input for the kinematic model of the DSEM (version 4.2 in Matlab 2014a, Mathworks). The data were recorded by Erik van de Graaff at the Amsterdam Arena using a marker-based optoelectronic method. Passive markers were used in combination with Vicon cameras with a sampling frequency of 100 Hz. The subjects were equipped with 10 markers on the following positions: spinous process of the 7th cervical vertebra (C7), incisura jugularis (IJ), xiphoid process (PX), spinous process of the eight thoracic vertebra (T8), cluster, medial humeral epicondyle (EM), lateral humeral epicondyle (EL), ulnar styloid US), radial styloid (UR), head of the third metacarpophalangeal joint (RHIP3) and the acromion (AC).

3D coordinates of the bony landmarks were filtered using a low-pass third order Butterworth filter with a cut-off frequency of 12.5 Hz. Joint angles were estimated from the marker coordinates for the following joints: thorax relative to global, the position of the IJ, clavicle relative to the thorax, humerus relative to the thorax, lower arm relative to the humerus and hand relative to the lower arm. The angles for the scapula relative to the thorax were estimated by using the initial orientation of the scapula relative to the clavicle of the DSEM and assuming that the scapula was fixed with respect to the clavicle during the motion.

The kinematic model of the DSEM was used to estimate the relative muscle length. A self-written algorithm, explained in Appendix 7.2, was used to remove outliers. The frames covering late-cocking phase until ball release were selected by selecting a period from 10 ms before until 5 ms after maximum external rotation. The average of the relative length of all muscle elements of each muscle over time was calculated to represent each muscle. The relative muscle velocity, in muscle lengths per second, was calculated from the muscle length by differentiating the muscle length with respect to time for each muscle. For all muscles, the length and velocity at maximum external rotation was calculated. For muscles that shorten more than 0.1 times the muscle length during the acceleration phase, the length at maximum external rotation and ball release was calculated. Mean values and standard deviations were calculated for these measures over the six different pitches.

For the length at maximum external rotation, muscles were categorized into three groups to describe their ability to produce force at that instant. Using the active force-length relationship in DSEM, relative muscle lengths were converted to maximum relative force, and the three groups were described by their percentage of maximum relative force: red (< 25%, or relative length of < 0.54 and > 1.44), green (>75%, or relative length of > 0.74 and < 1.20) and orange (25 – 75%, or in between red and green).

For the velocity at maximum external rotation, muscles are categorized into four groups to describe their ability to produce force at that instant. The groups were described by their relative velocity, a high negative velocity corresponds to the right hand side of the force-velocity curve, the maximum relative force is low: red (<-4ML/s), orange (-4 to -1 ML/s), green (-1 to 0 ML/s) and black (>0 ML/s, not shortening).

In all simulations the rotations of the thorax were set to zero, because the thorax rotations cause problems in the first kinematic step of the model. This is an issue that was already known to the research group.

4.3 RESULTS

Muscle length and velocity of 30 muscles was found for six pitches from four different subjects at maximum external rotation. At that point, the teres minor (0.41 ± 0.10) and infraspinatus (0.44 ± 0.05) had a very low relative muscle length and the serratus anterior (1.40 ± 0.12) and triceps caput longum (1.46 ± 0.05) had a very high relative length, all resulting in <25% of maximum relative force available (Table 11).

At maximum external rotation, the anconeus (-7.33 ± 0.74 ML/s), triceps (caput laterale: -6.80 ± 0.51, caput mediale: -6.20 ± 0.44, caput longum: -5.25 ± 0.77 ML/s) and serratus anterior (-4.05 ± 1.61 ML/s) had high velocities of <-4 ML/s, or shortening of over 4 ML/s (Table 12).

The aconeus (0.22), triceps (caput laterale: 0.22, caput longum 0.20, caput mediale: 0.20), serratus anterior (0.15), deltoideus pars scapularis (0.15) and supraspinatus (0.12) shortened more than 0.1 muscle length during acceleration (Table 13).

The muscle length relative to optimum length over time is shown for the pectoralis major, the triceps and the rotator cuff muscles in Figure 13: a-c. The muscle velocity, expressed in muscle lengths per second for the main scapular stabilizers (trapezius and serratus anterior), is shown in Figure 13d. The pectoralis major showed little length change. The triceps showed peak lengths just before maximum external rotation of the humerus and shortening after that. At maximum external rotation, the infraspinatus, teres minor and supraspinatus went from elongation to shortening and the subscapularis went from shortening to elongation. The trapezius elongated with a velocity between 0-3 ML/s. The serratus anterior shortened with a velocity over 4 ML/s.

Table 11: Relative muscle length at maximum external rotation

Muscle	L_{MER} (/optimum
Teres minor	0.41 ± 0.10
Infraspinatus	0.44 ± 0.05
Trapezius clavicular part	0.59 ± 0.05
Trapezius scapular part	0.67 ± 0.08
Latissimus dorsi	0.69 ± 0.03
Subscapularis	0.69 ± 0.04
Supraspinatus	0.76 ± 0.04
Rhomboideus	0.77 ± 0.03
Deltoideus	0.80 ± 0.04
Biceps caput longum proximal part	0.84 ± 0.02
Biceps caput longum distal part	0.84 ± 0.02
Anconeus	0.91 ± 0.02
Triceps caput laterale	0.96 ± 0.02
Pectoralis Minor	0.97 ± 0.06
Pronator teres ulna-radial	1.00 ± 0.06
Pronator quadratus	1.00 ± 0.10
Levator Scapulae	1.00 ± 0.03
Deltoideus clavicular part	1.00 ± 0.04
Triceps caput mediale	1.09 ± 0.02
Brachialis	1.09 ± 0.03
Brachioradialis	1.10 ± 0.04
Supinator ulna-radial	1.13 ± 0.04
Teres major	1.18 ± 0.04
Coracobrachialis	1.20 ± 0.03
Biceps caput breve	1.21 ± 0.06
Pronator teres humerus-radial	1.34 ± 0.04
Pectoralis major clavicular part	1.34 ± 0.01
Pectoralis major thoracic part	1.37 ± 0.02
Serratus anterior	1.40 ± 0.12
Triceps caput longum	1.46 ± 0.05

Table 12: Relative muscle velocity (ML/s) at maximum external rotation

Muscle	V_{MER} (ML/s)
Anconeus	-7.33 ± 0.74
Triceps caput laterale	-6.80 ± 0.51
Triceps caput mediale	-6.20 ± 0.44
Triceps caput longum	-5.25 ± 0.77
Serratus anterior	-4.05 ± 1.61
Teres minor	-1.98 ± 1.10
Supraspinatus	-1.72 ± 0.94
Pronator quadratus	-1.68 ± 1.52
Pronator teres ulna-radial	-1.36 ± 1.53
Levator Scapulae	-1.13 ± 0.67
Infraspinatus	-1.09 ± 0.71
Teres major	-0.94 ± 0.59
Pectoralis minor	-0.15 ± 0.77
Rhomboideus	-0.04 ± 0.71
Deltoideus scapular part	0.04 ± 0.41
Pectoralis major clavicular part	0.16 ± 0.18
Pectoralis major thoracic part	0.17 ± 0.49
Trapezius clavicular part	0.27 ± 0.78
Deltoideus clavicular part	0.69 ± 0.27
Coracobrachialis	0.76 ± 0.50
Subscapularis	0.85 ± 0.80
Latissimus dorsi	1.48 ± 0.97
Supinator ulna-radial	1.52 ± 1.25
Trapezius scapular part	2.33 ± 0.69
Pronator teres humerus-radial	4.08 ± 1.83
Brachialis	8.76 ± 0.19
Biceps caput longum distal part	9.21 ± 0.78
Biceps caput longum proximal part	9.21 ± 0.78
Brachioradialis	10.23 ± 0.58
Biceps caput breve	10.98 ± 1.02

Table 13: Muscles with >0.1 muscle length shortening during acceleration phase

Muscle	L_{MER} (/optimum length)	L_{BR} (/optimum length)
Anconeus	0.91 ± 0.02	0.69 ± 0.04
Triceps caput laterale	0.96 ± 0.02	0.74 ± 0.03
Triceps caput longum	1.46 ± 0.05	1.26 ± 0.03
Triceps caput mediale	1.09 ± 0.02	0.89 ± 0.03
Serratus anterior	1.40 ± 0.12	1.25 ± 0.06
Deltoideus pars scapularis	0.80 ± 0.04	0.65 ± 0.04
Supraspinatus	0.76 ± 0.04	0.64 ± 0.04

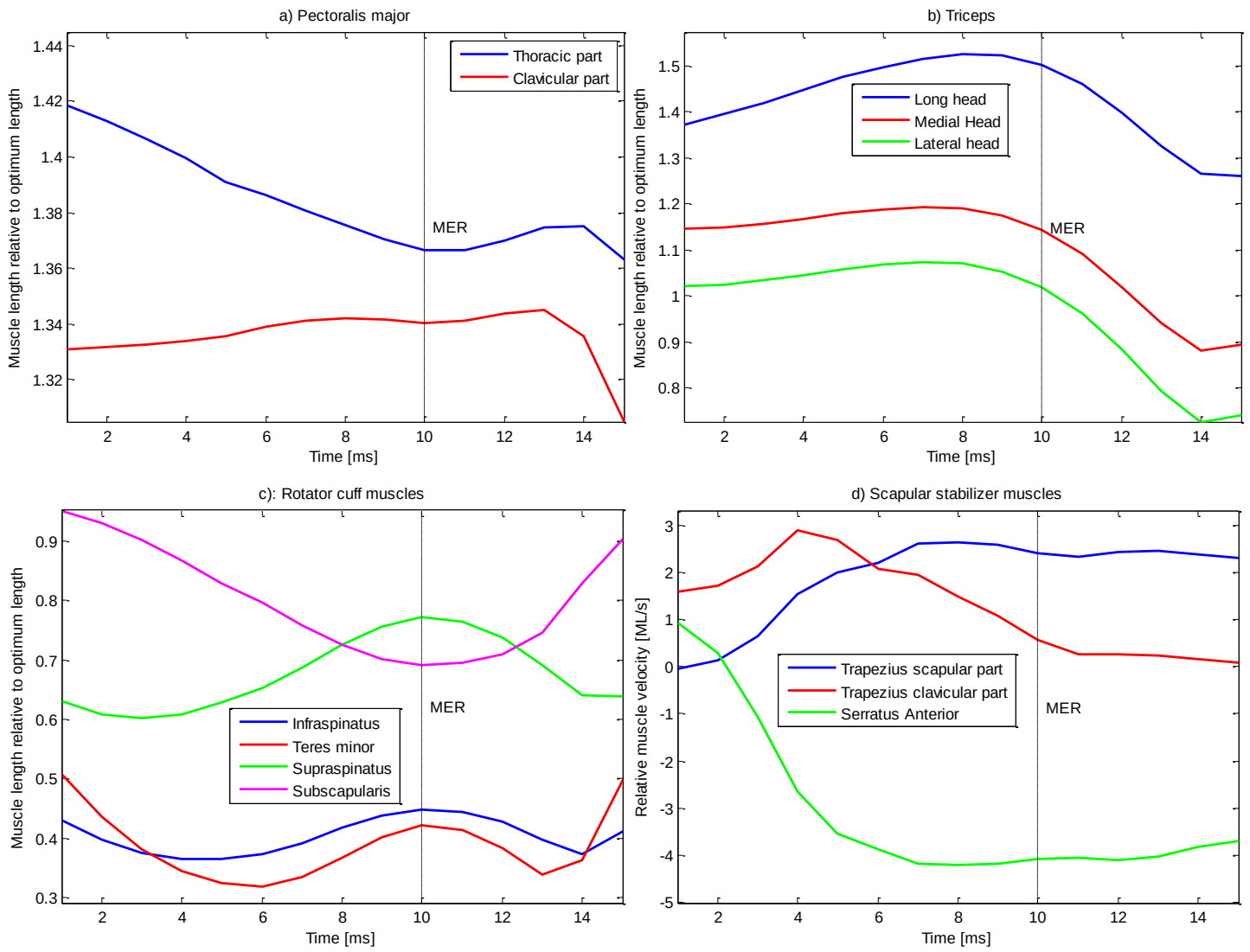

Figure 13: Relative muscle length for selected muscles from the late-cocking phase until ball release averaged over six pitches from four subjects. MER: maximum external rotation.

4.4 DISCUSSION

Muscle length and velocity were calculated for all muscles during the pitching motion to be able to compare these values to the force-velocity and the active force-length relationship, using red colors to mark muscles that are limited by one or both of these relationships to produce force. The teres minor, triceps (all three heads), infraspinatus, anconeus and serratus anterior fall into this category. Based on this, they are expected to have little active contribution to the accelerations of bones they attach to in the acceleration phase.

For elastic energy to be released and to significantly contribute to segment accelerations, a so-called 'stretch effect', it would be required that there is high shortening of muscles from the late-cocking to the acceleration phase. The muscles with shortening of > 0.1 were described in Table 13. However, elastic energy storage can only occur for stretched muscles. As the anconeus, triceps caput laterale, deltoideus pars scapularis and supraspinatus are below optimum length at maximum external rotation, no elastic energy can be stored. Triceps caput longum, triceps caput mediale and serratus anterior are stretched at maximum external rotation, so elastic energy could be stored and released for these muscles. The lengthening before shortening of the triceps is illustrated in Figure 13b. There is active lengthening before concentric contraction, since Jobe et al. (1984) found the activation as a percentage of maximum voluntary contraction of the triceps in the cocking and the acceleration phase to be 92% and 212% respectively. This was 88% and 55% respectively for the pectoralis major. However, Figure 13 shows little length change for the pectoralis major. Combining these findings leads to the conclusion that there is significant concentric contraction of the pectoralis major during the late-cocking and acceleration phase. This might be used to form a rigid connection between the thorax and the humerus, in order to be able to transfer energy from the thorax to the humerus. The rotator cuff muscles do not show a stretch effect (Figure 13c).

The results presented in this study should be interpreted carefully. As stated before, the angles for the scapula relative to the thorax were estimated by using the initial orientation of the scapula relative to the clavicle of the DSEM and assuming that the scapula was fixed during the motion. The sensitivity for the scapula angles is very high in the models, meaning that the rotation of the scapula has large influence on the moment arms and length of attaching muscles (Happee and Van der Helm, 1995, Charlton and Johnson, 2006). The muscles that will be affected by this are the muscles that attach to the scapula, like the trapezius and serratus anterior. Preferably, this research should be repeated with input kinematics with measured scapula angles instead of using an estimation using the initial orientation of the scapula relative to the clavicle of the DSEM and assuming that the scapula was fixed with respect to the clavicle during the motion.

Another factor to be considered is the fact that pitchers have developed adapted anatomical properties, as mentioned earlier in Chapter 2. For the humerus, maximum external rotation is increased and maximum internal rotation is decreased (Brown et al., 1988, Ellenbecker et al., 2002), so pitchers may have a larger optimum muscle length or a shifted working range. This would indicate that the relative muscle lengths and relative muscle velocities might be overestimated. Despite these reservations, it is reasonable to assume that the results give an indication of the ranges of the values and of the profiles of both length and velocity. To eliminate the possible effect of the shift in range of motion, this research should be repeated with pitchers where this shift in range of motion is not present.

Next steps after this research should be using a dynamic model to estimate muscle force and segment power during pitching. This will give more information on how the high accelerations in the pitching motion are achieved. This will require inclusion of the thorax angles, since the thorax plays a large role in force transfer during pitching.

5 Summary

A musculoskeletal model of the shoulder region, which uses kinematic data as an input an estimates muscle forces and joint loads as an output, can give valuable information on the pitching motion. This helps us to get more insight into the pitching motion and its biomechanical interactions and may also help in reducing the injury risk and increasing pitching velocity. Currently, there are three problems that impede proper simulations:

1. the lack of proper kinematic recordings
2. the fact that maximum force of the model could be too limited
3. the extreme character of the motion.

An experimental study was performed to create a dataset including upper limb kinematics and PCSA scaling factors to scale maximum force in the DSEM. An acromion cluster was used to track the scapula. PCSA scaling factors ranged from 1.11 to 2.02.

Following the experimental study, a case study was performed simulating this dataset in the DSEM. During simulation, the main problem arose in the optimization of the clavicle and scapula angles relative to the thorax, because the optimized angles contained large jumps, which are not realistic. This impeded proper simulation, because the jumps in muscle length caused both unsolved frames in the kinematics as well as in the dynamic model. Using a soft constraint instead of a hard constraint reduced these jumps and allowed for a complete solution in the kinematic model and an increase in the number of frames solved by the dynamic model. PCSA scaling also increased the number of frames solved by the dynamic model, however still unsolved frames were present, even after extreme scaling. Because of a change in range of motion as reported for pitchers, optimum muscle length might be different. This has a large impact in the model. If this would be the case, scaling optimum muscle length is recommended. In addition, segment scaling used in combination with using the soft constraint is recommended to improve the match between input angles and optimized angles, while still being compatible to the model.

To study the motion, the kinematic model of the DSEM was used to estimate muscle length and velocity for all muscles during the pitching motion. Comparing these values to the force-velocity and the active force-length relationship showed whether muscles were limited by one or both of these relationships to produce force. This was the case for the teres minor, triceps (all three heads), infraspinatus, anconeus and serratus anterior. The triceps showed a ‘stretch effect’, meaning shortening in the acceleration phase preceded by lengthening in the cocking phase. This means that there is a possibility for elastic energy to be stored for this muscle.

Applying the recommendations of this thesis will hopefully enable the dynamic model to perform a *complete* simulation of all frames with valid solutions. When this is accomplished, the next step might be to estimate muscle force and power during the pitching motion with the DSEM.

6 Bibliography

BAMMAN, M. M., NEWCOMER, B. R., LARSON-MEYER, D. E., WEINSIER, R. L. & HUNTER, G. R. 2000. Evaluation of the strength-size relationship in vivo using various muscle size indices. *Med Sci Sports Exerc,* 32**,** 1307-13.

BARNETT, N. D., DUNCAN, R. D. & JOHNSON, G. R. 1999. The measurement of three dimensional scapulohumeral kinematics--a study of reliability. *Clin Biomech (Bristol, Avon),* 14**,** 287-90.

BLEMKER, S. S., ASAKAWA, D. S., GOLD, G. E. & DELP, S. L. 2007. Image-based musculoskeletal modeling: Applications, advances, and future opportunities. *Journal of Magnetic Resonance Imaging,* 25**,** 441-451.

BOLSTERLEE, B., VARDY, A. N., VAN DER HELM, F. C. & VEEGER, H. E. 2015. The effect of scaling physiological cross-sectional area on musculoskeletal model predictions. *J Biomech,* 48**,** 1760-8.

BOLSTERLEE, B., VEEGER, H. E. J. & VAN DER HELM, F. C. T. 2014. Modelling clavicular and scapular kinematics: from measurement to simulation. *Medical & Biological Engineering & Computing,* 52**,** 283-291.

BRACKBILL, E., HALL, S., RICHARDS, J. & HAIGHT, J. 2007. A novel method of scapular tracking using tissue deformation. *Proceedings of the 12th annual GCMAS meeting*.

BROWN, L. P., NIEHUES, S. L., HARRAH, A., YAVORSKY, P. & HIRSHMAN, H. P. 1988. Upper extremity range of motion and isokinetic strength of the internal and external shoulder rotators in major league baseball players. *The American Journal of Sports Medicine,* 16**,** 577-585.

CAPPOZZO, A., CAPPELLO, A., DELLA CROCE, U. & PENSALFINI, F. 1997. Surface-marker cluster design criteria for 3-D bone movement reconstruction. *IEEE Trans Biomed Eng,* 44**,** 1165-74.

CHARLTON, I. W. & JOHNSON, G. R. 2006. A model for the prediction of the forces at the glenohumeral joint. *Proc Inst Mech Eng H,* 220**,** 801-12.

DAMSGAARD, M., RASMUSSEN, J., CHRISTENSEN, S. T., SURMA, E. & DE ZEE, M. 2006. Analysis of musculoskeletal systems in the AnyBody Modeling System. *Simulation Modelling Practice and Theory,* 14**,** 1100-1111.

DE GROOT, J. H. & BRAND, R. 2001. A three-dimensional regression model of the shoulder rhythm. *Clin Biomech (Bristol, Avon),* 16**,** 735-43.

DILLMAN, C. J., FLEISIG, G. S. & ANDREWS, J. R. 1993. Biomechanics of pitching with emphasis upon shoulder kinematics. *J Orthop Sports Phys Ther,* 18**,** 402-8.

DOWNAR, J. M. & SAUERS, E. L. 2005. Clinical Measures of Shoulder Mobility in the Professional Baseball Player. *Journal of Athletic Training,* 40**,** 23-29.

DUMAS, R., CHÈZE, L. & VERRIEST, J. P. 2007. Adjustments to McConville et al. and Young et al. body segment inertial parameters. *Journal of Biomechanics,* 40**,** 543-553.

EDMAN, K. A. 1979. The velocity of unloaded shortening and its relation to sarcomere length and isometric force in vertebrate muscle fibres. *The Journal of Physiology,* 291**,** 143-159.

ELLENBECKER, T. S., ROETERT, E. P., BAILIE, D. S., DAVIES, G. J. & BROWN, S. W. 2002. Glenohumeral joint total rotation range of motion in elite tennis players and baseball pitchers. *Med Sci Sports Exerc,* 34**,** 2052-6.

FLEISIG, G. S., BARRENTINE, S. W., ZHENG, N., ESCAMILLA, R. F. & ANDREWS, J. R. 1999. Kinematic and kinetic comparison of baseball pitching among various levels of development. *J Biomech,* 32**,** 1371-5.

FLEISIG, G. S., ESCAMILLA, R. F., ANDREWS, J. R., MATSUO, T., SATTERWHITE, Y. & BARRENTINE, S. W. 1996. Kinematic and kinetic comparison between baseball pitching and football passing. *Journal of Applied Biomechanics,* 12**,** 207-224.

FUKUNAGA, T., MIYATANI, M., TACHI, M., KOUZAKI, M., KAWAKAMI, Y. & KANEHISA, H. 2001. Muscle volume is a major determinant of joint torque in humans. *Acta Physiol Scand,* 172**,** 249-55.

GOMES, P. F., SESSELMANN, M., FARIA, C. D., ARAUJO, P. A. & TEIXEIRA-SALMELA, L. F. 2010. Measurement of scapular kinematics with the moire fringe projection technique. *J Biomech,* 43**,** 1215-9.

HAPPEE, R. & VAN DER HELM, F. C. 1995. The control of shoulder muscles during goal directed movements, an inverse dynamic analysis. *J Biomech,* 28**,** 1179-91.

HARRIS, R. I., VU, D. H., SONNABEND, D. H., GOLDBERG, J. A. & WALSH, W. R. 2001. Anatomic variance of the coracoclavicular ligaments. *Journal of Shoulder and Elbow Surgery,* 10**,** 585-588.

HILL, A. V. 1938. The Heat of Shortening and the Dynamic Constants of Muscle. *Proceedings of the Royal Society of London. Series B, Biological Sciences,* 126**,** 136-195.

HOLDEN, J. P., ORSINI, J. A., SIEGEL, K. L., KEPPLE, T. M., GERBER, L. H. & STANHOPE, S. J. 1997. Surface movement errors in shank kinematics and knee kinetics during gait. *Gait & Posture,* 5**,** 217-227.

HOLZBAUR, K. R., MURRAY, W. M. & DELP, S. L. 2005. A model of the upper extremity for simulating musculoskeletal surgery and analyzing neuromuscular control. *Ann Biomed Eng,* 33**,** 829-40.

JACQ, J. J., SCHWARTZ, C., BURDIN, V., GÉRARD, R., LEFÈVRE, C., ROUX, C. & RÉMY-NÉRIS, O. 2010. Building and Tracking Root Shapes. *IEEE*

Transactions on Biomedical Engineering, 57**,** 696-707.

JOBE, F. W., MOYNES, D. R., TIBONE, J. E. & PERRY, J. 1984. An EMG analysis of the shoulder in pitching. A second report. *Am J Sports Med,* 12**,** 218-20.

JOHNSON, G. R., STUART, P. R. & MITCHELL, S. 1993. A method for the measurement of three-dimensional scapular movement. *Clinical Biomechanics,* 8**,** 269-273.

KARDUNA, A. R., MCCLURE, P. W., MICHENER, L. A. & SENNETT, B. 2001. Dynamic measurements of three-dimensional scapular kinematics: a validation study. *J Biomech Eng,* 123**,** 184-90.

KARLSSON, D. & PETERSON, B. 1992. Towards a model for force predictions in the human shoulder. *J Biomech,* 25**,** 189-99.

KIBLER, W. B. 1998. The role of the scapula in athletic shoulder function. *Am J Sports Med,* 26**,** 325-37.

KROBOT, A., JANURA, M. & ELFMARK, M. 2009. Functional categorization of the individual morphology of the scapula. *Med Biol Eng Comput,* 47**,** 497-506.

LARSSON, L. & MOSS, R. L. 1993. Maximum velocity of shortening in relation to myosin isoform composition in single fibres from human skeletal muscles. *The Journal of Physiology,* 472**,** 595-614.

LEMPEREUR, M., BROCHARD, S., LEBOEUF, F. & RÉMY-NÉRIS, O. 2014. Validity and reliability of 3D marker based scapular motion analysis: A systematic review. *Journal of Biomechanics,* 47**,** 2219-2230.

LOPES, A. D., TIMMONS, M. K., GROVER, M., CICONELLI, R. M. & MICHENER, L. A. 2015. Visual Scapular Dyskinesis: Kinematics and Muscle Activity Alterations in Patients With Subacromial Impingement Syndrome. *Archives of Physical Medicine and Rehabilitation,* 96**,** 298-306.

MANDALIDIS, D. G., MC GLONE, B. S., QUIGLEY, R. F., MCINERNEY, D. & O'BRIEN, M. 1999. Digital fluoroscopic assessment of the scapulohumeral rhythm. *Surg Radiol Anat,* 21**,** 241-6.

MASJEDI, M. & JOHNSON, G. R. 2011. Alteration of scapula lateral rotation for subjects with the reversed anatomy shoulder replacement and its influence on glenohumeral joint contact force. *Proc Inst Mech Eng H,* 225**,** 38-47.

MESKERS, C. G. M., VAN DE SANDE, M. A. J. & DE GROOT, J. H. 2007. Comparison between tripod and skin-fixed recording of scapular motion. *Journal of Biomechanics,* 40**,** 941-946.

MESKERS, C. G. M., VERMEULEN, H. M., DE GROOT, J. H., VAN DER HELM, F. C. T. & ROZING, P. M. 1998. 3D shoulder position measurements using a six-degree-of-freedom electromagnetic tracking device. *Clinical Biomechanics,* 13**,** 280-292.

MORRIS, T. J., BRANDON, C. A., HORTON, M. J., CARLSON, D. S. & SCIOTE, J. J. 2001. Maximum Shortening Velocity and Myosin Heavy-chain Isoform Expression in Human Masseter Muscle Fibers. *Journal of dental research,* 80**,** 1845-1848.

MOYNES, D. R., PERRY, J., ANTONELLI, D. J. & JOBE, F. W. 1986. Electromyography and motion analysis of the upper extremity in sports. *Phys Ther,* 66**,** 1905-11.

MYERS, J. B., LAUDNER, K. G., PASQUALE, M. R., BRADLEY, J. P. & LEPHART, S. M. 2005. Scapular position and orientation in throwing athletes. *Am J Sports Med,* 33**,** 263-71.

NIKOOYAN, A. A., VEEGER, H. E., CHADWICK, E. K., PRAAGMAN, M. & HELM, F. C. 2011. Development of a comprehensive musculoskeletal model of the shoulder and elbow. *Med Biol Eng Comput,* 49**,** 1425-35.

NIKOOYAN, A. A., VEEGER, H. E., WESTERHOFF, P., GRAICHEN, F., BERGMANN, G. & VAN DER HELM, F. C. 2010. Validation of the Delft Shoulder and Elbow Model using in-vivo glenohumeral joint contact forces. *J Biomech,* 43**,** 3007-14.

PAPPAS, A. M., ZAWACKI, R. M. & SULLIVAN, T. J. 1985. Biomechanics of baseball pitching. *The American Journal of Sports Medicine,* 13**,** 216-222.

PRAAGMAN, M., CHADWICK, E. K. J., VAN DER HELM, F. C. T. & VEEGER, H. E. J. 2006. The relationship between two different mechanical cost functions and muscle oxygen consumption. *Journal of Biomechanics,* 39**,** 758-765.

PRINOLD, J. A. & BULL, A. M. 2016. Scapula kinematics of pull-up techniques: Avoiding impingement risk with training changes. *J Sci Med Sport,* 19**,** 629-35.

PRINOLD, J. A., MASJEDI, M., JOHNSON, G. R. & BULL, A. M. 2013. Musculoskeletal shoulder models: a technical review and proposals for research foci. *Proc Inst Mech Eng H,* 227**,** 1041-57.

PRINOLD, J. A., SHAHEEN, A. F. & BULL, A. M. 2011. Skin-fixed scapula trackers: a comparison of two dynamic methods across a range of calibration positions. *J Biomech,* 44**,** 2004-7.

PRINOLD, J. A. I. & BULL, A. M. J. 2014. Scaling and kinematics optimisation of the scapula and thorax in upper limb musculoskeletal models. *Journal of Biomechanics,* 47**,** 2813-2819.

REINSCHMIDT, C., VAN DEN BOGERT, A. J., NIGG, B. M., LUNDBERG, A. & MURPHY, N. 1997. Effect of skin movement on the analysis of skeletal knee joint motion during running. *J Biomech,* 30**,** 729-32.

SASAKI, K. & ISHII, N. 2005. Shortening velocity of human triceps surae muscle measured with the slack test in vivo. *The Journal of Physiology,* 567**,** 1047-1056.

SASAKI, K. & ISHII, N. 2010. Unloaded Shortening Velocity of Voluntarily and Electrically Activated Human Dorsiflexor Muscles In Vivo. *PLoS ONE,* 5**,** e13043.

SEROYER, S. T., NHO, S. J., BACH, B. R., BUSH-JOSEPH, C. A., NICHOLSON, G. P. & ROMEO, A. A. 2010. The Kinetic Chain in Overhand Pitching: Its Potential Role for Performance Enhancement and Injury Prevention. *Sports Health,* 2**,** 135-146.

SHAHEEN, A. F., ALEXANDER, C. M. & BULL, A. M. 2011. Effects of attachment position and shoulder orientation during calibration on the accuracy of the acromial tracker. *J Biomech,* 44**,** 1410-3.

TAKASE, K. 2010. The coracoclavicular ligaments: an anatomic study. *Surgical and Radiologic Anatomy,* 32**,** 683-688.

TALKHANI, I. S. & KELLY, C. P. 2001. Movement analysis of asymptomatic normal shoulders: a preliminary study. *J Shoulder Elbow Surg,* 10**,** 580-4.

VAN ANDEL, C., VAN HUTTEN, K., EVERSDIJK, M., VEEGER, D. & HARLAAR, J. 2009. Recording scapular motion using an acromion marker cluster. *Gait & Posture,* 29**,** 123-128.

VAN ANDEL, C. J., WOLTERBEEK, N., DOORENBOSCH, C. A. M., VEEGER, D. & HARLAAR, J. 2008. Complete 3D kinematics of upper extremity functional tasks. *Gait & Posture,* 27**,** 120-127.

VAN DER HELM, F. C., VEEGER, H. E., PRONK, G. M., VAN DER WOUDE, L. H. & ROZENDAL, R. H. 1992. Geometry parameters for musculoskeletal modelling of the shoulder system. *J Biomech,* 25**,** 129-44.

VEEGER, H. E., VAN DER HELM, F. C. & ROZENDAL, R. H. 1993. Orientation of the scapula in a simulated wheelchair push. *Clin Biomech (Bristol, Avon),* 8**,** 81-90.

VEEGER, H. E., YU, B., AN, K. N. & ROZENDAL, R. H. 1997. Parameters for modeling the upper extremity. *J Biomech,* 30**,** 647-52.

VIDT, M. E., DALY, M., MILLER, M. E., DAVIS, C. C., MARSH, A. P. & SAUL, K. R. 2012. Characterizing upper limb muscle volume and strength in older adults: a comparison with young adults. *J Biomech,* 45**,** 334-41.

WERNER, S. L., FLEISIG, G. S., DILLMAN, C. J. & ANDREWS, J. R. 1993. Biomechanics of the Elbow During Baseball Pitching. *Journal of Orthopaedic & Sports Physical Therapy,* 17**,** 274-278.

WOLFFSON, D. M. 1950. Scapula shape and muscle function, with special reference to the vertebral border. *American Journal of Physical Anthropology,* 8**,** 331-342.

WU, G., VAN DER HELM, F. C. T., VEEGER, H. E. J., MAKHSOUS, M., VAN ROY, P., ANGLIN, C., NAGELS, J., KARDUNA, A. R., MCQUADE, K., WANG, X., WERNER, F. W. & BUCHHOLZ, B. 2005. ISB recommendation on definitions of joint coordinate systems of various joints for the reporting of human joint motion—Part II: shoulder, elbow, wrist and hand. *Journal of Biomechanics,* 38**,** 981-992.

7 Appendices

7.1 FINDING SCALING FACTORS

This chapter describes how the maximum force of the subjects is obtained from the raw data. The data were filtered using a third order low-pass Butterworth filter with a cut-off frequency of 10 Hz. The raw force data, as shown in Figure 14 didn't have a unit. To convert the data to Newton, a calibration was performed. A weight of 5 kg was used to pull on the handle in three directions. The force that was applied was:

$$F = m * g = 5 * 9.81 = 49.05N$$

The peak value in the output of the force sensor in the direction of where the force was applied was divided by the external force in Newton. This was done for all six directions, resulting in six factors. The data from the force sensors was converted to Newton by multiplying each factor with the corresponding scaling factor.

To find the maximum force of the subject in each direction, the maximum and minimum value for each sensor was taken.

- For the sensor in x-direction, the minimum and maximum corresponded to right and left, respectively.
- For the sensor in y-direction, the minimum and maximum corresponded to down and up, respectively.
- For the sensor in z-direction, the minimum and maximum corresponded to pull and push, respectively.

The scaling factors, calculated from these maximum force values and the maximum force from the model, were implemented as follows: the anatomical data in the DSEM are stored in a so-called 'DSP file', that, besides from bony landmarks, ligaments, joint and segment definitions, stores the muscle definitions. These consist of geometric and muscle activation properties and the following muscle parameters: optimum fibre length, tendon length, pennation angle and PCSA. This file is called when running the model. The muscle parameters are then stored in a structure. The PCSA of the 139 muscle elements that make up the 30 muscles range from 0.16 to 5.10 cm^2. The muscle parameters from the DSP file are loaded at the beginning of simulation in DSEM. Among these muscle parameters that are loaded is a vector containing the PCSA values. Multiplying all elements in this vector by the scaling factor scales the PCSA of all muscles.

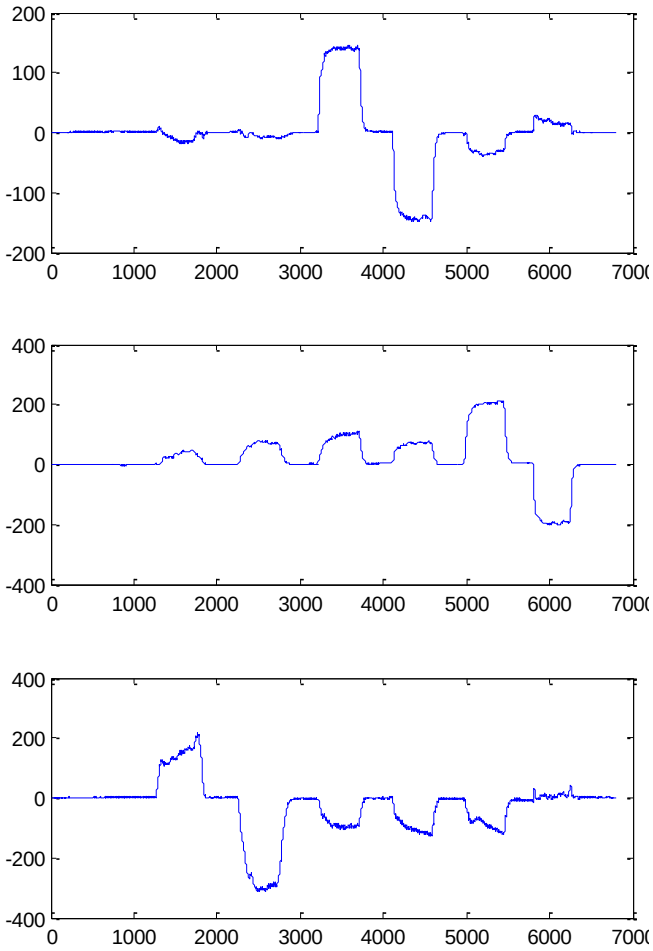

Figure 14: Raw data of the three force sensors, x-axis are samples (200 Hz), calibration is required to label y-axis

7.2 PROCESSING MUSCLE LENGTH

Muscle length relative to optimum length is a direct output of the simulations in DSEM; differentiation to a time vector directly results in the relative muscle velocity in muscle lengths per second. However, there are some instances where the muscle length makes a large jump for a few frames and then goes back (Figure 15a). This has big impact on the estimated muscle velocity (Figure 15b). This is clearly an artefact in the simulation and doesn't represent actual muscle function. The decision has been made to design an algorithm that removes these jumps in the muscle lengths and to interpolate these values.

To find jumps, absolute differences between subsequent values are calculated for the muscle lengths. Since jumps always occur in pairs (jump up then down, or the other way around), the frames of the jumps and the frames in-between are identified, their values removed and interpolated. The result can be seen in Figure 15a. The muscle velocity is still obtained by differentiating muscle length and didn't need further processing (Figure 15b).

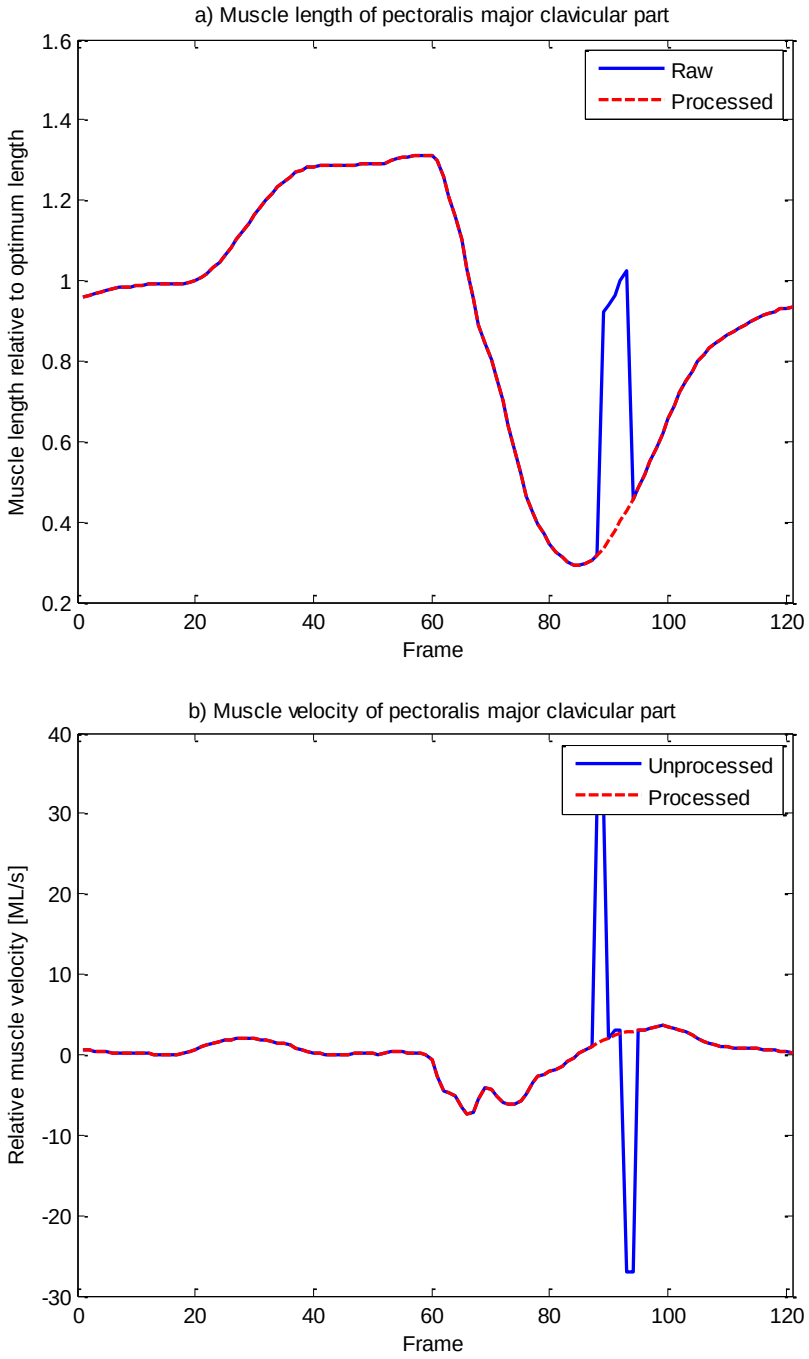

Figure 15: Correcting for muscle length jumps